Northumbria Research Link

Citation: Ghayesh, Mergen, Farokhi, Hamed and Farajpour, Ali (2019) Global dynamics of fluid conveying nanotubes. International Journal of Engineering Science, 135. pp. 37-57. ISSN 0020-7225

Published by: Elsevier

URL: http://dx.doi.org/10.1016/j.ijengsci.2018.11.003 <http://dx.doi.org/10.1016/j.ijengsci.2018.11.003>

This version was downloaded from Northumbria Research Link: http://nrl.northumbria.ac.uk/37451/

Northumbria University has developed Northumbria Research Link (NRL) to enable users to access the University's research output. Copyright © and moral rights for items on NRL are retained by the individual author(s) and/or other copyright owners. Single copies of full items can be reproduced, displayed or performed, and given to third parties in any format or medium for personal research or study, educational, or not-for-profit purposes without prior permission or charge, provided the authors, title and full bibliographic details are given, as well as a hyperlink and/or URL to the original metadata page. The content must not be changed in any way. Full items must not be sold commercially in any format or medium without formal permission of the copyright holder. The full policy is available online: http://nrl.northumbria.ac.uk/policies.html

This document may differ from the final, published version of the research and has been made available online in accordance with publisher policies. To read and/or cite from the published version of the research, please visit the publisher's website (a subscription may be required.)

Northumbria University NEWCASTLE

University Library

Global dynamics of fluid conveying nanotubes

Mergen H. Ghayesh [a*], Hamed Farokhi [b], Ali Farajpour [a]

[a] *School of Mechanical Engineering, University of Adelaide, South Australia 5005, Australia*
[b] *Department of Mechanical and Construction Engineering, Northumbria University, Newcastle upon Tyne NE1 8ST, UK*
[*] *Corresponding author's email: mergen.ghayesh@adelaide.edu.au*

Abstract

In the present article, an effort is made to analyse the coupled global dynamics of nanoscale fluid-conveying tubes. The influences of geometric nonlinearity are captured through the nonlinear Euler-Bernoulli strain relation of beams. Moreover, the size influences related to the nanoscale tube are captured via developing a nonlocal strain gradient model of beams. The Beskok-Karniadakis theory is also used for capturing the size influences related to the nanofluid. In addition to size influences, Coriolis acceleration effects together with the influences of the centrifugal acceleration are taken into account. Hamilton's principle gives two coupled equations of motions, which are discretised utilising Galerkin's technique. A time integration scheme is used for extracting the global dynamic characteristics of the nanotube containing nanofluid flow. The non-dimensional critical speed associated with buckling is also determined. It is found that the nanofluid speed plays a crucial role in the global dynamics in both the subcritical and supercritical regimes.

Keywords: Global dynamics; Nanoscale tubes; Nonlocal strain gradient model; nanoflow

1. Introduction

Many fluid-conveying ultrasmall systems with a variety of applications, especially in medicine, have recently been introduced [1, 2]. For instance, it has been shown that circulating tumour cells can be isolated from blood flow using a spiral microfluidics-based device [1]. In a fluid-conveying ultrasmall system, solid parts constantly interact with the fluid ones; the mechanical responses of the whole system are affected by these interactions. Predicting solid-fluid interactions is the key to better modelling and understanding of fluid-conveying systems at ultrasmall levels.

Since the mechanical response of ultrasmall systems is size-dependent [3-15], scale-free formulations based on the classical theory of elasticity are not reliable [16-37]. To develop a formulation capturing size influences, a few modified elasticity theories have been proposed to date [38-46]. The nonlocal strain gradient theory (NSGT) and the nonlocal elasticity theory (NET) are famous modified theories for nanoscale systems. The latter is utilised in this analysis for size influences.

The continuum-based analysis of fluid-conveying ultrasmall systems has attracted much attention in recent years. The most relevant continuum-based studies on these systems are discussed in the following. In one early investigation, a classical continuum-based analysis was conducted by Reddy et al. [47] for studying the free vibrations of single-walled carbon nanotubes (SWCNTs) containing nanofluid flow. Lee and Chang [48] scrutinised the vibrations of a fluid-conveying nanosystem using a SWCNT surrounded by an elastic medium. Moreover, Wang [49] extracted the dynamic characteristics of a double-walled carbon nanotube (DWCNT) conveying nanofluid incorporating nonlocal influences. Rafiei et al. [50] proposed a continuum-based formulation so as to explore the vibration of non-uniform nanotubes

containing nanofluid flow. Zhen and Fang [51] analysed the frequency response of nanoscale tubes conveying fluid via developing a nonlinear nonlocal model of elasticity; they modelled the size influences via help of one scale parameter. Rashidi et al. [52] examined the linear vibration of nanoscale tubes containing nanofluid flow; they took into account the size influence related to the fluid part. In another continuum-based analysis, Soltani et al. [53] studied the mechanical behaviours of nanofluid-conveying SWCNTs taking into account the influence of a surrounding viscoelastic medium. In another article, the influences of being geometrically curved along the longitudinal direction on the vibration response of nanotubes containing nanofluid flow are studied [54]. Li et al. [55] conducted a linear analysis based on the NSGT to extract the critical speeds of small-scale pipes containing nanofluid flow. In addition, a nonlinear NSGT-based model was proposed in the literature for studying the frequency response of nanoscale tubes conveying nanofluid [56]. Khosravian and Rafii-Tabar [57] also used the theory of Timoshenko beams for studying the motion of a multi-walled carbon nanotube (MWCNT) containing nanofluid flow. Hosseini and Sadeghi-Goughari [58] scrutinised the effects of a magnetic field along the axial direction on the mechanics of nanoscale tubes containing fluid flow. Similar continuum-based investigations have reported the mechanics of nanofluid-conveying piezoelectric nanotubes [59], boron nitride nanotubes [60] and functionally graded nanotubes [61].

Compared to linear vibration analysis and nonlinear frequency response analysis, few continuum-based analyses have reported the chaotic motions of nanotubes containing nanofluid flow [62]. However, to the best of our knowledge, size influences on the chaotic motions of nanofluid-conveying nanotubes have not been investigated yet. In this analysis, a nonlinear NSGT-based model of nanobeams is developed for capturing the geometric nonlinearity as well as the size influences related to the nanotube itself. The Beskok-

Karniadakis theory is employed to take into account size influences related to the nanofluid. Applying Hamilton's principle as a derivation scheme, the equations of motions along each direction are derived, leading to two coupled nonlinear differential equations. Utilising Galerkin's procedure and a time-integration-based solver, the coupled equations are simultaneously solved. The effects of external loads and nanofluid speed on the both subcritical and supercritical chaotic responses for the scale-dependent coupled motion of nanoscale tubes containing nanofluid flow are analysed and discussed.

2. A coupled NSGT-based model for chaos in fluid-conveying nanotubes

Employing the NSGT, a coupled nonlinear model of nanobeams is developed for investigating chaos in a nanotube of average diameter *d* and length *L* containing nanofluid flow (see Fig. 1). It is assumed that the nanotube has a constant cross-sectional area (*A*), constant elasticity modulus (*E*), and constant Poisson's ratio (*v*) (i.e. a uniform homogeneous nanotube). A harmonic load of amplitude *F*(*x*) and frequency ω is exerted on the nanotube (i.e. $\cos(\omega t)F(x)$) in the *z* direction. The mechanical strain is expressed as

$$\varepsilon_{xx} = e_{xx} + z\kappa_{xx}, \tag{1}$$

where

$$e_{xx} = \frac{\partial u}{\partial x} + \frac{1}{2}\left(\frac{\partial w}{\partial x}\right)^2, \quad \kappa_{xx} = -\frac{\partial^2 w}{\partial x^2}. \tag{2}$$

Here the displacement components of the mid-plane along the *x* and *z* axes are indicated by *u* and *w*, respectively. According to the NSGT, there three types of mechanical stresses: (1) zeroth-order nonlocal stress ($\sigma_{xx}^{(0)}$), (2) first-order nonlocal stress ($\sigma_{xx}^{(1)}$), and (3) total

mechanical stress ($\sigma_{xx}^{(t)}$). These stresses are related to the corresponding force and couple resultants as

$$\begin{aligned}
\left\langle N_{xx}^{(0)}, M_{xx}^{(0)} \right\rangle &= \int_A \left\langle \sigma_{xx}^{(0)}, z\sigma_{xx}^{(0)} \right\rangle dA, \\
\left\langle N_{xx}^{(1)}, M_{xx}^{(1)} \right\rangle &= \int_A \left\langle \sigma_{xx}^{(1)}, z\sigma_{xx}^{(1)} \right\rangle dA, \\
\left\langle N_{xx}^{(t)}, M_{xx}^{(t)} \right\rangle &= \int_A \left\langle \sigma_{xx}^{(t)}, z\sigma_{xx}^{(t)} \right\rangle dA.
\end{aligned} \tag{3}$$

Let us assume that the scale parameters associated with the stress nonlocality and strain gradients are, respectively, indicated by $\mu_n = e_0 \ell_n$ and $\mu_g = \ell_g$ in which e_0, ℓ_n and ℓ_g represent the calibration constant, internal characteristic length and strain gradient constant, respectively. The constitutive equation is given by

$$\sigma_{xx}^{(t)} - \mu_n^2 \nabla^2 \sigma_{xx}^{(t)} = E e_{xx} - E\mu_g^2 \nabla^2 e_{xx} + zE\kappa_{xx} - zE\mu_g^2 \nabla^2 \kappa_{xx}, \tag{4}$$

where ∇^2 is the Laplacian operator. Indicating the tube inertia moment by *I* and using Eq. (4), the corresponding force and couple resultants are as

$$N_{xx}^{(t)} - \mu_n^2 \nabla^2 N_{xx}^{(t)} = \frac{EA}{2}\left(\frac{\partial w}{\partial x}\right)^2 + EA\frac{\partial u}{\partial x} - EA\mu_g^2 \nabla^2 \left[\frac{1}{2}\left(\frac{\partial w}{\partial x}\right)^2 + \frac{\partial u}{\partial x}\right], \tag{5}$$

$$M_{xx}^{(t)} - \mu_n^2 \nabla^2 M_{xx}^{(t)} = -EI\frac{\partial^2 w}{\partial x^2} + EI\mu_g^2 \nabla^2 \frac{\partial^2 w}{\partial x^2}. \tag{6}$$

The variation of the elastic energy (U_{el}) is given by

$$\delta U_{el} = \int_0^L \int_A \sigma_{xx}^{(0)} \delta\varepsilon_{xx} dA dx + \int_0^L \int_A \sigma_{xx}^{(1)} \nabla \delta\varepsilon_{xx} dA dx, \tag{7}$$

where

$$\sigma_{xx}^{(t)} = \sigma_{xx}^{(0)} - \nabla \sigma_{xx}^{(1)}. \tag{8}$$

Here ∇ is the gradient operator. In addition, for the total kinetic energy (K_{en}) of the whole nanosystem, one can obtain

$$\begin{aligned}
\delta K_{en} &= m_{nt}\int_0^L \frac{\partial u}{\partial t}\delta\frac{\partial u}{\partial t}dx + m_{nt}\int_0^L \frac{\partial w}{\partial t}\delta\frac{\partial w}{\partial t}dx \\
&+ m_{nf}\int_0^L \left(\frac{\partial u}{\partial t} + \kappa_{BK}U\left(1+\frac{\partial u}{\partial x}\right)\right)\delta\frac{\partial u}{\partial t}dx \\
&+ m_{nf}\int_0^L \kappa_{BK}U\left(\frac{\partial u}{\partial t} + \kappa_{BK}U\left(1+\frac{\partial u}{\partial x}\right)\right)\delta\frac{\partial u}{\partial x}dx \\
&+ m_{nf}\int_0^L \left(\frac{\partial w}{\partial t} + \kappa_{BK}U\frac{\partial w}{\partial x}\right)\delta\frac{\partial w}{\partial t}dx \\
&+ m_{nf}\int_0^L \kappa_{BK}U\left(\frac{\partial w}{\partial t} + \kappa_{BK}U\frac{\partial w}{\partial x}\right)\delta\frac{\partial w}{\partial x}dx,
\end{aligned} \tag{9}$$

where m_{nt}, m_{nf} and U indicate the nanotube mass per length, nanofluid mass per length and the nanofluid speed, respectively; κ_{BK} denotes a correction factor related to the nanofluid speed. The size influences associated with the fluid part are incorporated into the formulation through this factor. Using Beskok-Karniadakis theory, one finally obtains the speed correction factor as

$$\kappa_{BK} = \left(\tau Kn + 1\right)\left[\frac{4Kn}{\left(1-\gamma Kn\right)}\left(\frac{2}{\eta}-1\right)+1\right], \tag{10}$$

where Kn denotes the Knudsen number; γ and η are two coefficients given by $\gamma = -1$ and $\eta = 0.7$, respectively; moreover, the coefficient τ is related to the Knudsen number as

$$\tau = \frac{2a_1}{\pi}\tan^{-1}\left[a_2\left(Kn\right)^{a_3}\right], \tag{11}$$

in which $a_1 = 64/\left(15\pi\right)$, $a_2 = 4$ and $a_3 = 0.4$. The external work (W_{ext}) is formulated as

$$\delta W_{ext} = \int_0^L \cos\left(\omega t\right)F\left(x\right)\delta w \, \mathrm{d}x. \tag{12}$$

Substituting Eqs. (7), (9) and (12) into the work/energy principle described by

$$\int_{t_1}^{t_2}\left(\delta K_{en}+\delta W_{ext}-\delta U_{el}\right)\mathrm{d}t=0, \tag{13}$$

the equations of motions are derived as

$$\frac{\partial N_{xx}^{(t)}}{\partial x}=\left(m_{nt}+m_{nf}\right)\frac{\partial^2 u}{\partial t^2}+2m_{nf}\kappa_{BK}U\frac{\partial^2 u}{\partial x\partial t}+m_{nf}\kappa_{BK}^2U^2\frac{\partial^2 u}{\partial x^2}, \tag{14}$$

$$\begin{aligned}&\frac{\partial^2 M_{xx}^{(t)}}{\partial x^2}+\frac{\partial}{\partial x}\left(N_{xx}^{(t)}\frac{\partial w}{\partial x}\right)+\cos\left(\omega t\right)F\left(x\right)=\\&\left(m_{nt}+m_{nf}\right)\frac{\partial^2 w}{\partial t^2}+2m_{nf}\kappa_{BK}U\frac{\partial^2 w}{\partial x\partial t}+m_{nf}\kappa_{BK}^2U^2\frac{\partial^2 w}{\partial x^2}.\end{aligned} \tag{15}$$

Eqs. (5) and (6) are used together with Eqs. (14) and (15), resulting in the following equations of motions in terms of *u* and *w*

$$\begin{aligned}&\left(m_{nt}+m_{nf}\right)\frac{\partial^2 u}{\partial t^2}+2m_{nf}\kappa_{BK}U\frac{\partial^2 u}{\partial t\partial x}+m_{nf}\kappa_{BK}^2U^2\frac{\partial^2 u}{\partial x^2}\\&-\mu_n^2\left[\left(m_{nt}+m_{nf}\right)\frac{\partial^4 u}{\partial x^2\partial t^2}+2m_{nf}\kappa_{BK}U\frac{\partial^4 u}{\partial t\partial x^3}+m_{nf}\kappa_{BK}^2U^2\frac{\partial^4 u}{\partial x^4}\right]\\&-EA\frac{\partial}{\partial x}\left[\frac{1}{2}\left(\frac{\partial w}{\partial x}\right)^2+\frac{\partial u}{\partial x}\right]+EA\mu_g^2\frac{\partial^3}{\partial x^3}\left[\frac{1}{2}\left(\frac{\partial w}{\partial x}\right)^2+\frac{\partial u}{\partial x}\right]=0,\end{aligned} \tag{16}$$

$$\begin{aligned}&-EI\frac{\partial^4 w}{\partial x^4}+EI\mu_g^2\frac{\partial^6 w}{\partial x^6}+\cos\left(\omega t\right)F\left(x\right)-\mu_n^2\cos\left(\omega t\right)\frac{\partial^2 F\left(x\right)}{\partial x^2}\\&+EA\frac{\partial^2 w}{\partial x^2}\left(\frac{\partial u}{\partial x}+\frac{1}{2}\left(\frac{\partial w}{\partial x}\right)^2-\mu_g^2\frac{\partial^2}{\partial x^2}\left[\frac{\partial u}{\partial x}+\frac{1}{2}\left(\frac{\partial w}{\partial x}\right)^2\right]\right)\\&+EA\frac{\partial w}{\partial x}\left(\frac{\partial^2 u}{\partial x^2}+\frac{\partial^2 w}{\partial x^2}\frac{\partial w}{\partial x}-\mu_g^2\frac{\partial^2}{\partial x^2}\left(\frac{\partial^2 u}{\partial x^2}+\frac{\partial^2 w}{\partial x^2}\frac{\partial w}{\partial x}\right)\right)\\&+\mu_n^2\frac{\partial^2 w}{\partial x^2}\left[\left(m_{nt}+m_{nf}\right)\frac{\partial^3 u}{\partial x\partial t^2}+2m_{nf}\kappa_{BK}U\frac{\partial^3 u}{\partial x^2\partial t}+m_{nf}\kappa_{BK}^2U^2\frac{\partial^3 u}{\partial x^3}\right]\\&+\mu_n^2\frac{\partial w}{\partial x}\left[\left(m_{nt}+m_{nf}\right)\frac{\partial^4 u}{\partial x^2\partial t^2}+2m_{nf}\kappa_{BK}U\frac{\partial^4 u}{\partial x^3\partial t}+m_{nf}\kappa_{BK}^2U^2\frac{\partial^4 u}{\partial x^4}\right]\end{aligned}$$

$$
\begin{aligned}
&-\mu_n^2\frac{\partial^2}{\partial x^2}\left\{EA\frac{\partial^2 w}{\partial x^2}\left(\frac{\partial u}{\partial x}+\frac{1}{2}\left(\frac{\partial w}{\partial x}\right)^2-\mu_g^2\frac{\partial^2}{\partial x^2}\left[\frac{\partial u}{\partial x}+\frac{1}{2}\left(\frac{\partial w}{\partial x}\right)^2\right]\right)\right.\\
&+EA\frac{\partial w}{\partial x}\left(\frac{\partial^2 u}{\partial x^2}+\frac{\partial^2 w}{\partial x^2}\frac{\partial w}{\partial x}-\mu_g^2\frac{\partial^2}{\partial x^2}\left(\frac{\partial^2 u}{\partial x^2}+\frac{\partial^2 w}{\partial x^2}\frac{\partial w}{\partial x}\right)\right)\\
&+\mu_n^2\frac{\partial^2 w}{\partial x^2}\left[\left(m_{nt}+m_{nf}\right)\frac{\partial^3 u}{\partial x\partial t^2}+2m_{nf}\kappa_{BK}U\frac{\partial^3 u}{\partial x^2\partial t}+m_{nf}\kappa_{BK}^2U^2\frac{\partial^3 u}{\partial x^3}\right]\\
&\left.+\mu_n^2\frac{\partial w}{\partial x}\left[\left(m_{nt}+m_{nf}\right)\frac{\partial^4 u}{\partial x^2\partial t^2}+2m_{nf}\kappa_{BK}U\frac{\partial^4 u}{\partial x^3\partial t}+m_{nf}\kappa_{BK}^2U^2\frac{\partial^4 u}{\partial x^4}\right]\right\}\\
&=\left(m_{nt}+m_{nf}\right)\frac{\partial^2 w}{\partial t^2}+2m_{nf}\kappa_{BK}U\frac{\partial^2 w}{\partial x\partial t}+m_{nf}\kappa_{BK}^2U^2\frac{\partial^2 w}{\partial x^2}\\
&-\mu_n^2\left[\left(m_{nt}+m_{nf}\right)\frac{\partial^4 w}{\partial x^2\partial t^2}+2m_{nf}\kappa_{BK}U\frac{\partial^4 w}{\partial x^3\partial t}+m_{nf}\kappa_{BK}^2U^2\frac{\partial^4 w}{\partial x^4}\right].
\end{aligned}
\tag{17}
$$

Let us define a set of non-dimensional parameters as follows

$$
\begin{aligned}
&x^*=\frac{x}{L},\ u^*=\frac{u}{2R_o},\ w^*=\frac{w}{2R_o},\ \alpha=\frac{AL^2}{I},\ \beta=\frac{L}{2R_o},\\
&\bar{\mu}_n=\frac{\mu_n}{L},\ \bar{\mu}_g=\frac{\mu_g}{L},\ \omega^*=\omega\sqrt{\frac{L^4\left(m_{nt}+m_{nf}\right)}{EI}},\ U^*=U\sqrt{\frac{m_{nf}L^2}{EI}},\\
&\Gamma_m=\frac{m_{nf}}{m_{nt}+m_{nf}},\ t^*=t\sqrt{\frac{EI}{L^4\left(m_{nt}+m_{nf}\right)}},\ F^*=\frac{FL^4}{2R_oEI},
\end{aligned}
\tag{18}
$$

where R_o is the nanotube outer radius. Employing Eq. (18) and assuming a constant forcing amplitude, the non-dimensional coupled motion equations are derived as

$$
\begin{aligned}
&\frac{\beta}{\alpha}\left[\frac{\partial^2 u}{\partial t^2}+2\kappa_{BK}\sqrt{\Gamma_m}U\frac{\partial^2 u}{\partial t\partial x}+\kappa_{BK}^2U^2\frac{\partial^2 u}{\partial x^2}\right]\\
&-\frac{\beta}{\alpha}\bar{\mu}_n^2\frac{\partial^2}{\partial x^2}\left[\frac{\partial^2 u}{\partial t^2}+2\kappa_{BK}\sqrt{\Gamma_m}U\frac{\partial^2 u}{\partial t\partial x}+\kappa_{BK}^2U^2\frac{\partial^2 u}{\partial x^2}\right]\\
&-\frac{\partial}{\partial x}\left[\frac{1}{2}\left(\frac{\partial w}{\partial x}\right)^2+\beta\frac{\partial u}{\partial x}\right]+\bar{\mu}_g^2\frac{\partial^3}{\partial x^3}\left[\frac{1}{2}\left(\frac{\partial w}{\partial x}\right)^2+\beta\frac{\partial u}{\partial x}\right]=0,
\end{aligned}
\tag{19}
$$

$$
\begin{aligned}
&-\bar{\mu}_g^2\frac{\partial^6 w}{\partial x^6}+\frac{\partial^4 w}{\partial x^4}-\cos(\omega t)F_1+\frac{\partial^2 w}{\partial t^2}+\kappa_{BK}^2U^2\frac{\partial^2 w}{\partial x^2}+2\kappa_{BK}\sqrt{\Gamma_m}U\frac{\partial^2 w}{\partial x\partial t}\\
&-\bar{\mu}_n^2\left[\frac{\partial^4 w}{\partial x^2\partial t^2}+\kappa_{BK}^2U^2\frac{\partial^4 w}{\partial x^4}+2\kappa_{BK}\sqrt{\Gamma_m}U\frac{\partial^4 w}{\partial t\partial x^3}\right]\\
&-\frac{\alpha}{\beta^2}\left\{\frac{\partial^2 w}{\partial x^2}\left(\frac{1}{2}\left(\frac{\partial w}{\partial x}\right)^2+\beta\frac{\partial u}{\partial x}-\bar{\mu}_g^2\frac{\partial^2}{\partial x^2}\left[\frac{1}{2}\left(\frac{\partial w}{\partial x}\right)^2+\beta\frac{\partial u}{\partial x}\right]\right)\right.\\
&+\frac{\partial w}{\partial x}\left(\frac{\partial w}{\partial x}\frac{\partial^2 w}{\partial x^2}+\beta\frac{\partial^2 u}{\partial x^2}-\bar{\mu}_g^2\frac{\partial^2}{\partial x^2}\left(\frac{\partial w}{\partial x}\frac{\partial^2 w}{\partial x^2}+\beta\frac{\partial^2 u}{\partial x^2}\right)\right)\\
&+\frac{\beta}{\alpha}\bar{\mu}_n^2\frac{\partial^2 w}{\partial x^2}\left[\frac{\partial^3 u}{\partial x\partial t^2}+\kappa_{BK}^2U^2\frac{\partial^3 u}{\partial x^3}+2\kappa_{BK}\sqrt{\Gamma_m}U\frac{\partial^3 u}{\partial t\partial x^2}\right]\\
&\left.+\frac{\beta}{\alpha}\bar{\mu}_n^2\frac{\partial w}{\partial x}\left[\frac{\partial^4 u}{\partial x^2\partial t^2}+\kappa_{BK}^2U^2\frac{\partial^4 u}{\partial x^4}+2\kappa_{BK}\sqrt{\Gamma_m}U\frac{\partial^4 u}{\partial t\partial x^3}\right]\right\}\\
&+\frac{\alpha}{\beta^2}\bar{\mu}_n^2\frac{\partial^2}{\partial x^2}\left\{\frac{\partial^2 w}{\partial x^2}\left(\frac{1}{2}\left(\frac{\partial w}{\partial x}\right)^2+\beta\frac{\partial u}{\partial x}-\bar{\mu}_g^2\frac{\partial^2}{\partial x^2}\left[\frac{1}{2}\left(\frac{\partial w}{\partial x}\right)^2+\beta\frac{\partial u}{\partial x}\right]\right)\right.\\
&+\frac{\partial w}{\partial x}\left(\frac{\partial w}{\partial x}\frac{\partial^2 w}{\partial x^2}+\beta\frac{\partial^2 u}{\partial x^2}-\bar{\mu}_g^2\frac{\partial^2}{\partial x^2}\left(\frac{\partial w}{\partial x}\frac{\partial^2 w}{\partial x^2}+\beta\frac{\partial^2 u}{\partial x^2}\right)\right)\\
&+\frac{\beta}{\alpha}\bar{\mu}_n^2\frac{\partial^2 w}{\partial x^2}\left[\frac{\partial^3 u}{\partial x\partial t^2}+\kappa_{BK}^2U^2\frac{\partial^3 u}{\partial x^3}+2\kappa_{BK}\sqrt{\Gamma_m}U\frac{\partial^3 u}{\partial t\partial x^2}\right]\\
&\left.+\frac{\beta}{\alpha}\bar{\mu}_n^2\frac{\partial w}{\partial x}\left[\frac{\partial^4 u}{\partial x^2\partial t^2}+\kappa_{BK}^2U^2\frac{\partial^4 u}{\partial x^4}+2\kappa_{BK}\sqrt{\Gamma_m}U\frac{\partial^4 u}{\partial t\partial x^3}\right]\right\}=0.
\end{aligned}
\tag{20}
$$

To discretise Eqs. (19) and (20), the following expressions are utilised

$$
\begin{Bmatrix}u(x,t)\\ w(x,t)\end{Bmatrix}=\begin{Bmatrix}\sum_{j=1}^{N_x}r_j(t)\varphi_j^{(u)}(x)\\ \sum_{j=1}^{N_z}q_j(t)\varphi_j^{(w)}(x)\end{Bmatrix},
\tag{21}
$$

where $r_j(t)$, $\varphi_j^{(u)}(x)$, $q_j(t)$ and $\varphi_j^{(w)}(x)$ represent the axial generalised coordinates, axial trial functions, transverse generalised coordinates and transverse trial functions, respectively. Substituting Eq. (21) into Eqs. (19) and (20) and using Galerkin's technique, one derives

$$\frac{\beta}{\alpha}\left[\sum_{j=1}^{N_x}\frac{d^2r_j}{dt^2}\left(\int_0^1\varphi_k^{(u)}\varphi_j^{(u)}dx\right)+2\kappa_{BK}\sqrt{\Gamma_m}U\sum_{j=1}^{N_x}\frac{dr_j}{dt}\left(\int_0^1\varphi_k^{(u)}\frac{d\varphi_j^{(u)}}{dx}dx\right)\right.$$
$$\left.+\kappa_{BK}^2U^2\sum_{j=1}^{N_x}r_j\left(\int_0^1\varphi_k^{(u)}\frac{d^2\varphi_j^{(u)}}{dx^2}dx\right)\right]-\frac{\beta}{\alpha}\bar{\mu}_n^2\left[\sum_{j=1}^{N_x}\frac{d^2r_j}{dt^2}\left(\varphi_k^{(u)}\int_0^1\frac{d^2\varphi_j^{(u)}}{dx^2}dx\right)\right.$$
$$\left.+2\kappa_{BK}\sqrt{\Gamma_m}U\sum_{j=1}^{N_x}\frac{dr_j}{dt}\left(\int_0^1\varphi_k^{(u)}\frac{d^3\varphi_j^{(u)}}{dx^3}dx\right)+\kappa_{BK}^2U^2\sum_{j=1}^{N_x}r_j\left(\int_0^1\varphi_k^{(u)}\frac{d^4\varphi_j^{(u)}}{dx^4}dx\right)\right] \tag{22}$$
$$-\int_0^1\varphi_k^{(u)}\frac{d}{dx}\left[\frac{1}{2}\left(\sum_{j=1}^{N_z}q_j\frac{d\varphi_j^{(w)}}{dx}\right)^2+\beta\sum_{j=1}^{N_x}r_j\frac{d\varphi_j^{(u)}}{dx}\right]dx$$
$$+\bar{\mu}_g^2\int_0^1\varphi_k^{(u)}\frac{d^3}{dx^3}\left[\frac{1}{2}\left(\sum_{j=1}^{N_z}q_j\frac{d\varphi_j^{(w)}}{dx}\right)^2+\beta\sum_{j=1}^{N_x}r_j\frac{d\varphi_j^{(u)}}{dx}\right]dx=0,$$

$$\sum_{j=1}^{N_z}\frac{d^2q_j}{dt^2}\left(\int_0^1\varphi_k^{(w)}\varphi_j^{(w)}dx\right)+2\kappa_{BK}\sqrt{\Gamma_m}U\sum_{j=1}^{N_z}\frac{dq_j}{dt}\left(\int_0^1\varphi_k^{(w)}\frac{d\varphi_j^{(w)}}{dx}dx\right)$$
$$+\kappa_{BK}^2U^2\sum_{j=1}^{N_z}q_j\left(\int_0^1\varphi_k^{(w)}\frac{d^2\varphi_j^{(w)}}{dx^2}dx\right)-\bar{\mu}_n^2\left[\sum_{j=1}^{N_z}\frac{d^2q_j}{dt^2}\left(\int_0^1\varphi_k^{(w)}\frac{d^2\varphi_j^{(w)}}{dx^2}dx\right)\right.$$
$$\left.+2\kappa_{BK}\sqrt{\Gamma_m}U\sum_{j=1}^{N_z}\frac{dq_j}{dt}\left(\int_0^1\varphi_k^{(w)}\frac{d^3\varphi_j^{(w)}}{dx^3}dx\right)+\kappa_{BK}^2U^2\sum_{j=1}^{N_z}q_j\left(\int_0^1\varphi_k^{(w)}\frac{d^4\varphi_j^{(w)}}{dx^4}dx\right)\right]$$
$$-\bar{\mu}_g^2\sum_{j=1}^{N_z}q_j\left(\int_0^1\varphi_k^{(w)}\frac{d^6\varphi_j^{(w)}}{dx^6}dx\right)+\sum_{j=1}^{N_z}q_j\left(\int_0^1\varphi_k^{(w)}\frac{d^4\varphi_j^{(w)}}{dx^4}dx\right)-\left(\int_0^1\varphi_k^{(w)}dx\right)\cos(\omega t)F_1$$
$$-\frac{\alpha}{\beta^2}\int_0^1\left\{\varphi_k^{(w)}\left[\left(\sum_{j=1}^{N_z}q_j\frac{d^2\varphi_j^{(w)}}{dx^2}\right)\left(\frac{1}{2}\sum_{i=1}^{N_z}\sum_{j=1}^{N_z}q_iq_j\frac{d\varphi_j^{(w)}}{dx}\frac{d\varphi_i^{(w)}}{dx}+\beta\sum_{j=1}^{N_x}r_j\frac{d\varphi_j^{(u)}}{dx}\right.\right.\right.$$
$$\left.\left.\left.-\bar{\mu}_g^2\frac{d^2}{dx^2}\left(\frac{1}{2}\sum_{i=1}^{N_z}\sum_{j=1}^{N_z}q_iq_j\frac{d\varphi_j^{(w)}}{dx}\frac{d\varphi_i^{(w)}}{dx}+\beta\sum_{j=1}^{N_x}r_j\frac{d\varphi_j^{(u)}}{dx}\right)\right)\right.$$
$$+\left(\sum_{j=1}^{N_z}q_j\frac{d\varphi_j^{(w)}}{dx}\right)\left(\sum_{i=1}^{N_z}\sum_{j=1}^{N_z}q_iq_j\frac{d\varphi_j^{(w)}}{dx}\frac{d^2\varphi_i^{(w)}}{dx^2}+\beta\sum_{j=1}^{N_x}r_j\frac{d^2\varphi_j^{(u)}}{dx^2}\right.$$
$$\left.-\bar{\mu}_g^2\frac{d^2}{dx^2}\left(\sum_{i=1}^{N_z}\sum_{j=1}^{N_z}q_iq_j\frac{d\varphi_j^{(w)}}{dx}\frac{d^2\varphi_i^{(w)}}{dx^2}+\beta\sum_{j=1}^{N_x}r_j\frac{d^2\varphi_j^{(u)}}{dx^2}\right)\right)$$
$$+\frac{\beta\bar{\mu}_n^2}{\alpha}\left(\sum_{j=1}^{N_z}q_j\frac{d^2\varphi_j^{(w)}}{dx^2}\right)\left(\sum_{j=1}^{N_x}\frac{d^2r_j}{dt^2}\frac{d\varphi_j^{(u)}}{dx}+\kappa_{BK}^2U^2\sum_{j=1}^{N_x}r_j\frac{d^3\varphi_j^{(u)}}{dx^3}+2\kappa_{BK}\sqrt{\Gamma_m}U\sum_{j=1}^{N_x}\frac{dr_j}{dt}\frac{d^2\varphi_j^{(u)}}{dx^2}\right)$$
$$\left.\left.+\frac{\beta\bar{\mu}_n^2}{\alpha}\left(\sum_{j=1}^{N_z}q_j\frac{d\varphi_j^{(w)}}{dx}\right)\left(\sum_{j=1}^{N_x}\frac{d^2r_j}{dt^2}\frac{d^2\varphi_j^{(u)}}{dx^2}+\kappa_{BK}^2U^2\sum_{j=1}^{N_x}r_j\frac{d^4\varphi_j^{(u)}}{dx^4}+2\kappa_{BK}\sqrt{\Gamma_m}U\sum_{j=1}^{N_x}\frac{dr_j}{dt}\frac{d^3\varphi_j^{(u)}}{dx^3}\right)\right]\right\}dx$$

$$
\begin{aligned}
&+\frac{\alpha\bar{\mu}_n^2}{\beta^2}\int_0^1\Bigg\{\varphi_k^{(w)}\frac{d^2}{dx^2}\Bigg[\left(\sum_{j=1}^{N_z}q_j\frac{d^2\varphi_j^{(w)}}{dx^2}\right)\left(\frac{1}{2}\sum_{i=1}^{N_z}\sum_{j=1}^{N_z}q_iq_j\frac{d\varphi_j^{(w)}}{dx}\frac{d\varphi_i^{(w)}}{dx}+\beta\sum_{j=1}^{N_x}r_j\frac{d\varphi_j^{(u)}}{dx}\right.\\
&\left.-\bar{\mu}_g^2\frac{d^2}{dx^2}\left(\frac{1}{2}\sum_{i=1}^{N_z}\sum_{j=1}^{N_z}q_iq_j\frac{d\varphi_j^{(w)}}{dx}\frac{d\varphi_i^{(w)}}{dx}+\beta\sum_{j=1}^{N_x}r_j\frac{d\varphi_j^{(u)}}{dx}\right)\right)\\
&+\left(\sum_{j=1}^{N_z}q_j\frac{d\varphi_j^{(w)}}{dx}\right)\left(\sum_{i=1}^{N_z}\sum_{j=1}^{N_z}q_iq_j\frac{d\varphi_j^{(w)}}{dx}\frac{d^2\varphi_i^{(w)}}{dx^2}+\beta\sum_{j=1}^{N_x}r_j\frac{d^2\varphi_j^{(u)}}{dx^2}\right.\\
&\left.-\bar{\mu}_g^2\frac{d^2}{dx^2}\left(\sum_{i=1}^{N_z}\sum_{j=1}^{N_z}q_iq_j\frac{d\varphi_j^{(w)}}{dx}\frac{d^2\varphi_i^{(w)}}{dx^2}+\beta\sum_{j=1}^{N_x}r_j\frac{d^2\varphi_j^{(u)}}{dx^2}\right)\right)\\
&+\frac{\beta\bar{\mu}_n^2}{\alpha}\left(\sum_{j=1}^{N_z}q_j\frac{d^2\varphi_j^{(w)}}{dx^2}\right)\left(\sum_{j=1}^{N_x}\frac{d^2r_j}{dt^2}\frac{d\varphi_j^{(u)}}{dx}+\kappa_{BK}^2U^2\sum_{j=1}^{N_x}r_j\frac{d^3\varphi_j^{(u)}}{dx^3}+2\kappa_{BK}\sqrt{\Gamma_m}U\sum_{j=1}^{N_x}\frac{dr_j}{dt}\frac{d^2\varphi_j^{(u)}}{dx^2}\right)\\
&+\frac{\beta\bar{\mu}_n^2}{\alpha}\left(\sum_{j=1}^{N_z}q_j\frac{d\varphi_j^{(w)}}{dx}\right)\left(\sum_{j=1}^{N_x}\frac{d^2r_j}{dt^2}\frac{d^2\varphi_j^{(u)}}{dx^2}+\kappa_{BK}^2U^2\sum_{j=1}^{N_x}r_j\frac{d^4\varphi_j^{(u)}}{dx^4}+2\kappa_{BK}\sqrt{\Gamma_m}U\sum_{j=1}^{N_x}\frac{dr_j}{dt}\frac{d^3\varphi_j^{(u)}}{dx^3}\right)\Bigg]\Bigg\}=0,
\end{aligned}
\tag{23}
$$

Equations (22) and (23) gives a number of ordinary differential equations, which are solved via a time-integration-based solver.

3. Numerical results

The nanosystem mechanical properties are assumed as E=610 MPa and v=0.3. Furthermore, the nanosystem geometric properties are assumed as h=70.0 nm, R_o=230.0 nm and L/d_{out}=20. The non-dimensional values of the nanosystem are as κ_{BK}=1.10, Γ_m=0.4780, β=20.0, α = 4312.8662, $\bar{\mu}_g = 0.04$ and $\bar{\mu}_n = 0.08$. In numerical calculations, a damping ratio of 0.005 is utilised. Ten degrees of freedom (DOF) are considered for each displacement component, resulting in a system of 20 DOF.

The non-dimensional critical speed associated with buckling is 5.2214. The coupled bifurcation response is first plotted in Fig. 2 for U = 5.05, highlighting the subcritical response of the nanosystem. Different motion types are seen in this figure. The coupled motion is

periodic for $0 < F_1 < 9$ while a period-3 coupled motion is seen for $9 \leq F_1 < 9.5$. Then a region of periodic motion is observed followed by some other types of motions. In particular, a number of quasiperiodic motions are found for $40 < F_1 < 50$. For clarification purposes, more details about the nanosystem motion at F_1= 20.0 and F_1= 42.7 are also given in Figs. 3 and 4, respectively. At F_1= 20.0, the nanotube experiences a periodic motion while it displays a quasiperiodic motion at F_1= 42.7.

Figure 5 depicts the coupled bifurcation of the nanotube containing nanofluid flow of non-dimensional speed U =5.10 (i.e. a bit higher nanofluid speed) for both w and u. Comparing Figs. 2 and 5 reveals that the coupled bifurcation response is greatly dependent on the nanofluid speed. For example, the coupled motion is periodic at F_1= 5.5 for U = 5.05 while it is a period-3 type at this forcing amplitude for U =5.10. Figure 6 is plotted to give more details about the coupled motion of the nanosystem described in Fig. 5 at F_1= 25. It is concluded that the nanoscale tube containing nanofluid flow displays a period-3 coupled motion at this forcing amplitude.

A further increase in the speed of the nanofluid flow results in a completely different bifurcation response, as shown in Fig. 7. This indicates the significance of the nanofluid speed in the bifurcation response of nanoscale tubes containing nanofluid flow. There is noticeable chaos in the coupled motion, especially for specific values of the forcing amplitude between F_1= 30 and F_1= 50. With increasing nanofluid speed from U = 5.15 to U = 5.20, the chaos in the coupled motion significantly spreads over a wider range of the forcing amplitude. This means that just before the critical point in the subcritical regime, the nanofluid speed plays a crucial role in the coupled chaotic response. Figures 9 and 10, respectively, indicate the details of the coupled motions of the nanotube containing nanofluid flow, which is described in Fig. 8, at

F_1= 25 and F_1= 38. From these figures, it is seen that the nanosystem experiences periodic and chaotic motions at F_1= 25 and F_1= 38, respectively.

Similar to the subcritical regime, the influences of the nanofluid speed together with the forcing amplitude on the bifurcation response of the nanotube containing nanofluid flow are also scrutinised in the supercritical one. The coupled bifurcation response of the nanosystem is first plotted in Fig. 11 for U = 5.25. It is found that the coupled motion is highly chaotic a bit beyond the critical point. Figure 12 gives more details about the chaotic motion of the nanoscale tube at F_1= 46.

Figure 13 illustrates the influence of a slight increase in the nanofluid speed on the coupled bifurcation of the nanotube containing nanofluid flow (U = 5.30). Comparing this figure with the previous bifurcation response plotted in Fig. 11 reveals that the interval of F_1 in which the nanotube experiences a chaotic motion decreases when the nanofluid speed is increased in the supercritical regime. However, significant chaos is still observed in the coupled bifurcation response (see Fig. 14). Furthermore, Fig. 15 illustrates the coupled bifurcation of the nanotube containing nanofluid flow of U= 5.40 for both w and u, indicating a further reduction in the interval of F_1 in which chaos happens.

4. Conclusions

The chaotic motions of nanofluid-conveying nanoscale tubes have been investigated via developing a nonlinear NSGT-based model of nanobeams. The geometric nonlinearity and size influence related to the nanotube were captured employing the nonlinear strain relation and the NSGT, respectively. Furthermore, the size influence related to the nanofluid was taken into account employing the Beskok-Karniadakis theory. Applying Hamilton's principle led to two coupled nonlinear differential equations for the nanosystem. The coupled equations were simultaneously solved by utilising a time-integration-based solver as well as Galerkin's procedure.

In addition to periodic and period-3 coupled motions, the nanotube experiences a number of quasiperiodic motions in the subcritical regime for specific values of nanofluid speed and forcing amplitude. There is noticeable chaos in the coupled motion of the nanotube containing nanofluid flow near the critical point corresponding to buckling. In the subcritical regime, as the nanofluid speed increases, chaos in the coupled motion spreads over a wider range of the forcing amplitude. It was also found that a bit beyond the critical point, the coupled motions of the nanosystem are highly chaotic. However, in the supercritical regime, as the nanofluid speed increases, the interval of the forcing amplitude in which the nanosystem experiences a chaotic response reduces.

References

[1] M.E. Warkiani, G. Guan, K.B. Luan, W.C. Lee, A.A.S. Bhagat, P.K. Chaudhuri, D.S.-W. Tan, W.T. Lim, S.C. Lee, P.C. Chen, Slanted spiral microfluidics for the ultra-fast, label-free isolation of circulating tumor cells, Lab on a Chip, 14 (2014) 128-137.

[2] A.M. Dehrouyeh-Semnani, M. Nikkhah-Bahrami, M.R.H. Yazdi, On nonlinear stability of fluid-conveying imperfect micropipes, International Journal of Engineering Science, 120 (2017) 254-271.

[3] M. Mojahedi, Size dependent dynamic behavior of electrostatically actuated microbridges, International Journal of Engineering Science, 111 (2017) 74-85.

[4] L. Qi, S. Huang, G. Fu, S. Zhou, X. Jiang, On the mechanics of curved flexoelectric microbeams, International Journal of Engineering Science, 124 (2018) 1-15.

[5] H. Farokhi, M.H. Ghayesh, Nonlinear mechanics of electrically actuated microplates, International Journal of Engineering Science, 123 (2018) 197-213.

[6] M.H. Ghayesh, H. Farokhi, M. Amabili, Nonlinear behaviour of electrically actuated MEMS resonators, International Journal of Engineering Science, 71 (2013) 137-155.

[7] M.H. Ghayesh, H. Farokhi, G. Alici, Size-dependent performance of microgyroscopes, International Journal of Engineering Science, 100 (2016) 99-111.

[8] H. Farokhi, M.H. Ghayesh, M. Amabili, Nonlinear dynamics of a geometrically imperfect microbeam based on the modified couple stress theory, International Journal of Engineering Science, 68 (2013) 11-23.

[9] S. Khakalo, V. Balobanov, J. Niiranen, Modelling size-dependent bending, buckling and vibrations of 2D triangular lattices by strain gradient elasticity models: Applications to sandwich beams and auxetics, International Journal of Engineering Science, 127 (2018) 33-52.

[10] H. Farokhi, M.H. Ghayesh, Nonlinear mechanical behaviour of microshells, International Journal of Engineering Science, 127 (2018) 127-144.

[11] M.A. Attia, A.A. Abdel Rahman, On vibrations of functionally graded viscoelastic nanobeams with surface effects, International Journal of Engineering Science, 127 (2018) 1-32.

[12] E. Taati, On buckling and post-buckling behavior of functionally graded micro-beams in thermal environment, International Journal of Engineering Science, 128 (2018) 63-78.

[13] S. Srividhya, P. Raghu, A. Rajagopal, J.N. Reddy, Nonlocal nonlinear analysis of functionally graded plates using third-order shear deformation theory, International Journal of Engineering Science, 125 (2018) 1-22.

[14] M.H. Ghayesh, Functionally graded microbeams: Simultaneous presence of imperfection and viscoelasticity, International Journal of Mechanical Sciences, 140 (2018) 339-350.

[15] M.H. Ghayesh, Nonlinear vibration analysis of axially functionally graded shear-deformable tapered beams, Applied Mathematical Modelling, 59 (2018) 583-596.

[16] M.H. Ghayesh, H. Farokhi, A. Gholipour, Oscillations of functionally graded microbeams, International Journal of Engineering Science, 110 (2017) 35-53.

[17] M.H. Ghayesh, H. Farokhi, Global dynamics of imperfect axially forced microbeams, International Journal of Engineering Science, 68 (2017) 188-202.

[18] H. Farokhi, M.H. Ghayesh, A. Gholipour, S. Hussain, Motion characteristics of bilayered extensible Timoshenko microbeams, International Journal of Engineering Science, 112 (2017) 1-17.

[19] H. Farokhi, M.H. Ghayesh, A. Gholipour, Dynamics of functionally graded micro-cantilevers, International Journal of Engineering Science, 115 (2017) 117-130.

[20] H. Farokhi, M.H. Ghayesh, A. Gholipour, M. Tavallaeinejad, Nonlinear oscillations of viscoelastic microplates, International Journal of Engineering Science, 118 (2017) 56-69.

[21] M.H. Ghayesh, H. Farokhi, A. Gholipour, S. Hussain, On the nonlinear mechanics of layered microcantilevers, International Journal of Engineering Science, 120 (2017) 1-14.

[22] M.H. Ghayesh, H. Farokhi, Nonlinear mechanics of doubly curved shallow microshells, International Journal of Engineering Science, 119 (2017) 288-304.

[23] M.H. Ghayesh, H. Farokhi, A. Gholipour, M. Tavallaeinejad, Nonlinear bending and forced vibrations of axially functionally graded tapered microbeams, International Journal of Engineering Science, 120 (2017) 51-62.
[24] H. Farokhi, M.H. Ghayesh, A. Gholipour, M. Tavallaeinejad, Nonlinear oscillations of viscoelastic microplates, International Journal of Engineering Science, 118 (2017) 56-69.
[25] Ç. Demir, Ö. Civalek, On the analysis of microbeams, International Journal of Engineering Science, 121 (2017) 14-33.
[26] M. Rahaeifard, M. Mojahedi, On the mechanics of laminated microplates, International Journal of Engineering Science, 119 (2017) 180-188.
[27] A.M. Dehrouyeh-Semnani, On boundary conditions for thermally loaded FG beams, International Journal of Engineering Science, 119 (2017) 109-127.
[28] M.A. Attia, On the mechanics of functionally graded nanobeams with the account of surface elasticity, International Journal of Engineering Science, 115 (2017) 73-101.
[29] G.-L. She, F.-G. Yuan, Y.-R. Ren, W.-S. Xiao, On buckling and postbuckling behavior of nanotubes, International Journal of Engineering Science, 121 (2017) 130-142.
[30] S. Rajasekaran, H.B. Khaniki, Bending, buckling and vibration of small-scale tapered beams, International Journal of Engineering Science, 120 (2017) 172-188.
[31] H. Shahverdi, M.R. Barati, Vibration analysis of porous functionally graded nanoplates, International Journal of Engineering Science, 120 (2017) 82-99.
[32] X.-J. Xu, M.-L. Zheng, X.-C. Wang, On vibrations of nonlocal rods: Boundary conditions, exact solutions and their asymptotics, International Journal of Engineering Science, 119 (2017) 217-231.
[33] L. Medina, R. Gilat, S. Krylov, Latching in bistable electrostatically actuated curved micro beams, International Journal of Engineering Science, 110 (2017) 15-34.
[34] H. Bakhshi Khaniki, S. Hosseini-Hashemi, Dynamic response of biaxially loaded double-layer viscoelastic orthotropic nanoplate system under a moving nanoparticle, International Journal of Engineering Science, 115 (2017) 51-72.
[35] S. Seyedkavoosi, D. Zaytsev, B. Drach, P. Panfilov, M. Yu. Gutkin, I. Sevostianov, Fraction-exponential representation of the viscoelastic properties of dentin, International Journal of Engineering Science, 111 (2017) 52-60.
[36] H. Shahverdi, M.R. Barati, Vibration analysis of porous functionally graded nanoplates, International Journal of Engineering Science, 120 (2017) 82-99.
[37] M.H. Ghayesh, Dynamics of functionally graded viscoelastic microbeams, International Journal of Engineering Science, 124 (2018) 115-131.
[38] M.H. Ghayesh, H. Farokhi, A. Gholipour, M. Tavallaeinejad, Nonlinear oscillations of functionally graded microplates, International Journal of Engineering Science, 122 (2018) 56-72.
[39] H.B. Khaniki, On vibrations of nanobeam systems, International Journal of Engineering Science, 124 (2018) 85-103.
[40] R. Bahaadini, A.R. Saidi, M. Hosseini, On dynamics of nanotubes conveying nanoflow, International Journal of Engineering Science, 123 (2018) 181-196.
[41] L. Li, H. Tang, Y. Hu, The effect of thickness on the mechanics of nanobeams, International Journal of Engineering Science, 123 (2018) 81-91.
[42] R. Barretta, M. Čanađija, R. Luciano, F.M. de Sciarra, Stress-driven modeling of nonlocal thermoelastic behavior of nanobeams, International Journal of Engineering Science, 126 (2018) 53-67.
[43] A.M. Dehrouyeh-Semnani, On the thermally induced non-linear response of functionally graded beams, International Journal of Engineering Science, 125 (2018) 53-74.
[44] M.H. Ghayesh, H. Farokhi, M. Amabili, Nonlinear dynamics of a microscale beam based on the modified couple stress theory, Composites Part B: Engineering, 50 (2013) 318-324.
[45] M.H. Ghayesh, H. Farokhi, On the viscoelastic dynamics of fluid-conveying microtubes, International Journal of Engineering Science, 127 (2018) 186-200.
[46] M.H. Ghayesh, A. Farajpour, Nonlinear mechanics of nanoscale tubes via nonlocal strain gradient theory, International Journal of Engineering Science, 129 (2018) 84-95.

[47] C. Reddy, C. Lu, S. Rajendran, K. Liew, Free vibration analysis of fluid-conveying single-walled carbon nanotubes, Applied Physics Letters, 90 (2007) 133122.
[48] H.-L. Lee, W.-J. Chang, Free transverse vibration of the fluid-conveying single-walled carbon nanotube using nonlocal elastic theory, Journal of Applied Physics, 103 (2008) 024302.
[49] L. Wang, Dynamical behaviors of double-walled carbon nanotubes conveying fluid accounting for the role of small length scale, Computational Materials Science, 45 (2009) 584-588.
[50] M. Rafiei, S.R. Mohebpour, F. Daneshmand, Small-scale effect on the vibration of non-uniform carbon nanotubes conveying fluid and embedded in viscoelastic medium, Physica E: Low-Dimensional Systems and Nanostructures, 44 (2012) 1372-1379.
[51] Y.-X. Zhen, B. Fang, Nonlinear vibration of fluid-conveying single-walled carbon nanotubes under harmonic excitation, International Journal of Non-Linear Mechanics, 76 (2015) 48-55.
[52] V. Rashidi, H.R. Mirdamadi, E. Shirani, A novel model for vibrations of nanotubes conveying nanoflow, Computational Materials Science, 51 (2012) 347-352.
[53] P. Soltani, M. Taherian, A. Farshidianfar, Vibration and instability of a viscous-fluid-conveying single-walled carbon nanotube embedded in a visco-elastic medium, Journal of Physics D: Applied Physics, 43 (2010) 425401.
[54] W. Xia, L. Wang, Vibration characteristics of fluid-conveying carbon nanotubes with curved longitudinal shape, Computational Materials Science, 49 (2010) 99-103.
[55] L. Li, Y. Hu, X. Li, L. Ling, Size-dependent effects on critical flow velocity of fluid-conveying microtubes via nonlocal strain gradient theory, Microfluidics and Nanofluidics, 20 (2016) 76.
[56] A. Farajpour, H. Farokhi, M.H. Ghayesh, S. Hussain, Nonlinear mechanics of nanotubes conveying fluid, International Journal of Engineering Science, 133 (2018) 132-143.
[57] N. Khosravian, H. Rafii-Tabar, Computational modelling of a non-viscous fluid flow in a multi-walled carbon nanotube modelled as a Timoshenko beam, Nanotechnology, 19 (2008) 275703.
[58] M. Hosseini, M. Sadeghi-Goughari, Vibration and instability analysis of nanotubes conveying fluid subjected to a longitudinal magnetic field, Applied Mathematical Modelling, 40 (2016) 2560-2576.
[59] Z. Saadatnia, E. Esmailzadeh, Nonlinear harmonic vibration analysis of fluid-conveying piezoelectric-layered nanotubes, Composites Part B: Engineering, 123 (2017) 193-209.
[60] A.G. Arani, M. Bagheri, R. Kolahchi, Z.K. Maraghi, Nonlinear vibration and instability of fluid-conveying DWBNNT embedded in a visco-Pasternak medium using modified couple stress theory, Journal of Mechanical Science and Technology, 27 (2013) 2645-2658.
[61] S. Filiz, M. Aydogdu, Wave propagation analysis of embedded (coupled) functionally graded nanotubes conveying fluid, Composite Structures, 132 (2015) 1260-1273.
[62] W. Hu, Z. Deng, Chaos in embedded fluid-conveying single-walled carbon nanotube under transverse harmonic load series, Nonlinear Dynamics, 79 (2015) 325-333.

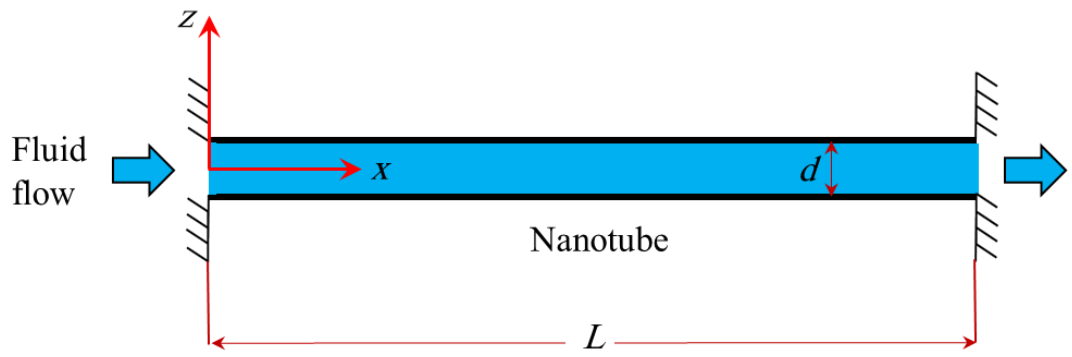

Fig. 1. A nanotube of average diameter *d* and length *L* containing fluid flow.

(a)

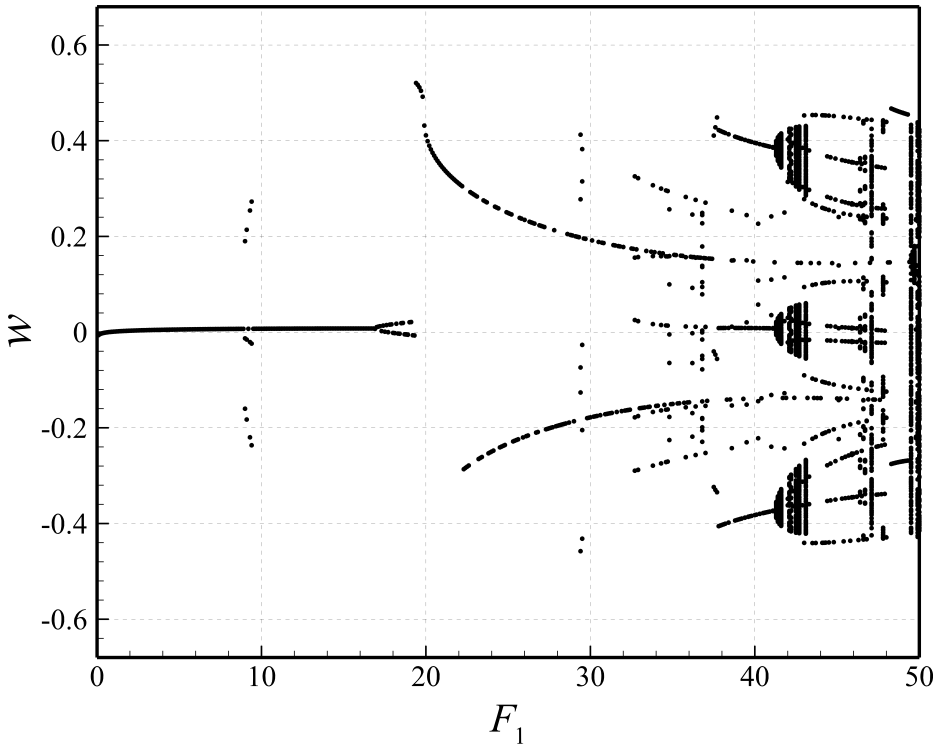

(b)

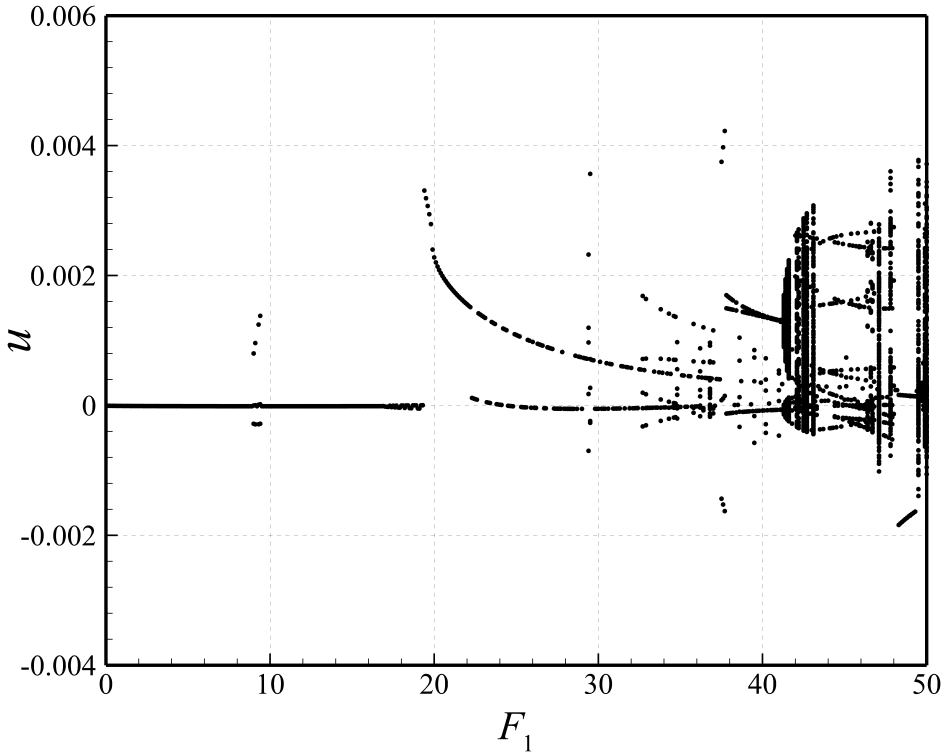

Figure 2: Coupled bifurcation response of the nanoscale tube containing nanofluid flow of speed U = 5.05 for (a) $w(x=0.50)$ and (b) $u(x=0.65)$; ω_1= 4.5217 and ω/ω_1=1.0.

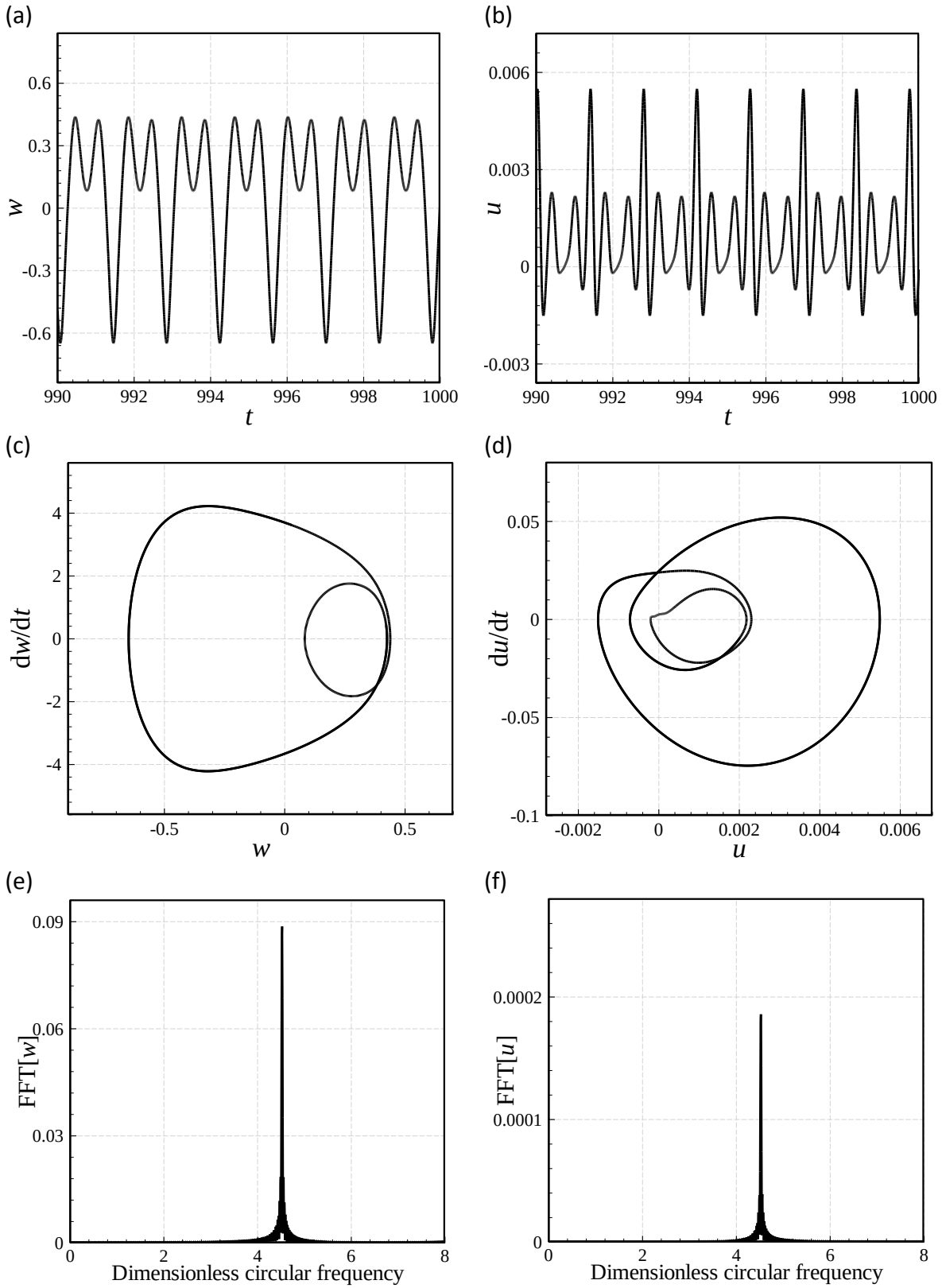

Figure 3: More details about the nanosystem motion (described in Fig. 2) at F_1=20.0: (a) $w(x=0.5)$ versus time, (b) $u(x=0.65)$ versus time, (c) $dw/dt(x=0.5)$ versus transverse displacement, (d) $du/dt(x=0.65)$ versus axial displacement, (e) FFT for $w(x=0.5)$, and (f) FFT for $u(x=0.65)$.

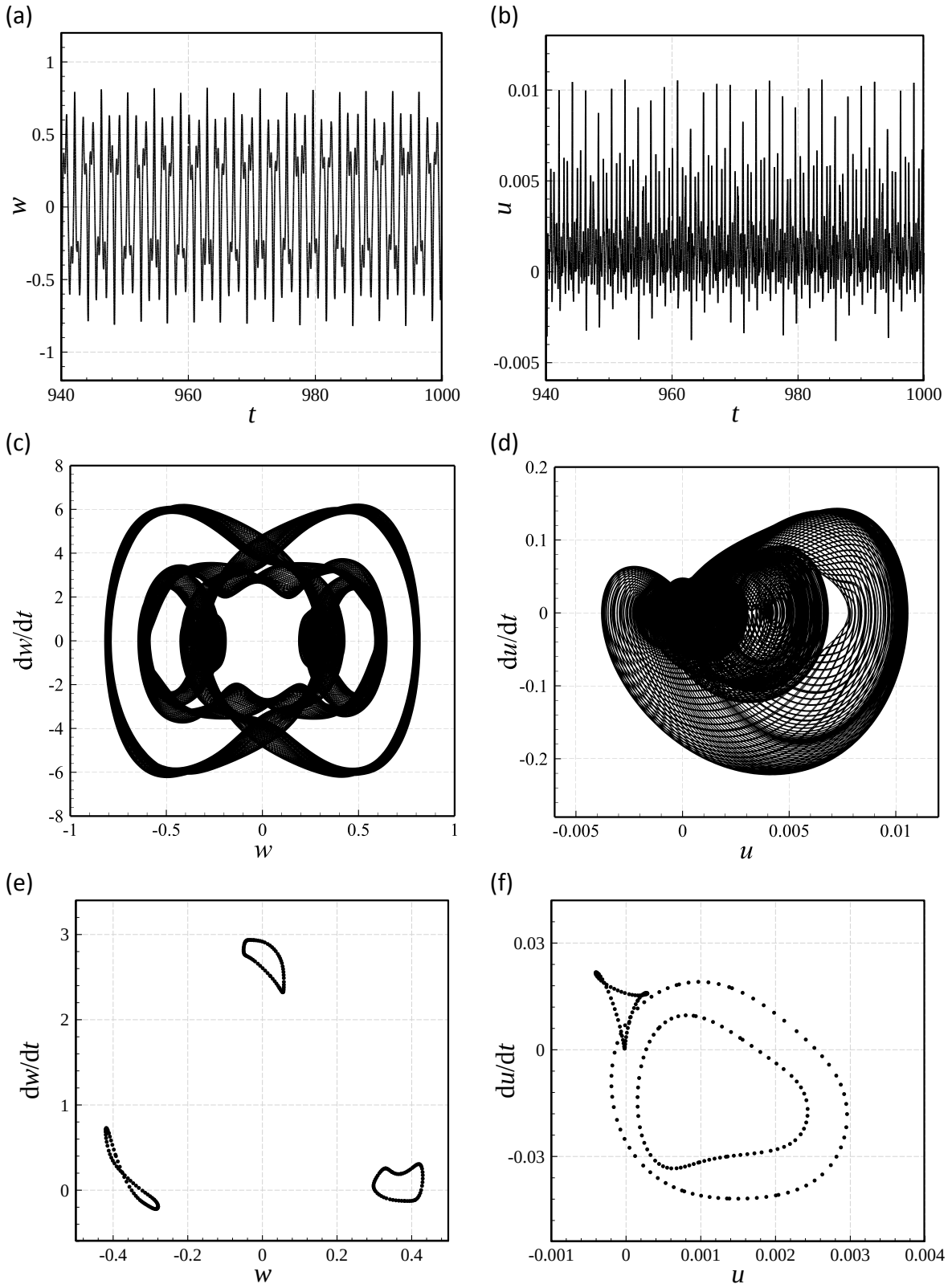

Figure 4: More details about the nanosystem motion (described in Fig. 2) at F_1=42.7: (a) $w(x=0.5)$ versus time, (b) $u(x=0.65)$ versus time, (c) $dw/dt(x=0.5)$ versus transverse displacement, (d) $du/dt(x=0.65)$ versus axial displacement, (e) Poincaré map for $w(x=0.5)$, and (f) Poincaré map for $u(x=0.65)$.

(a)

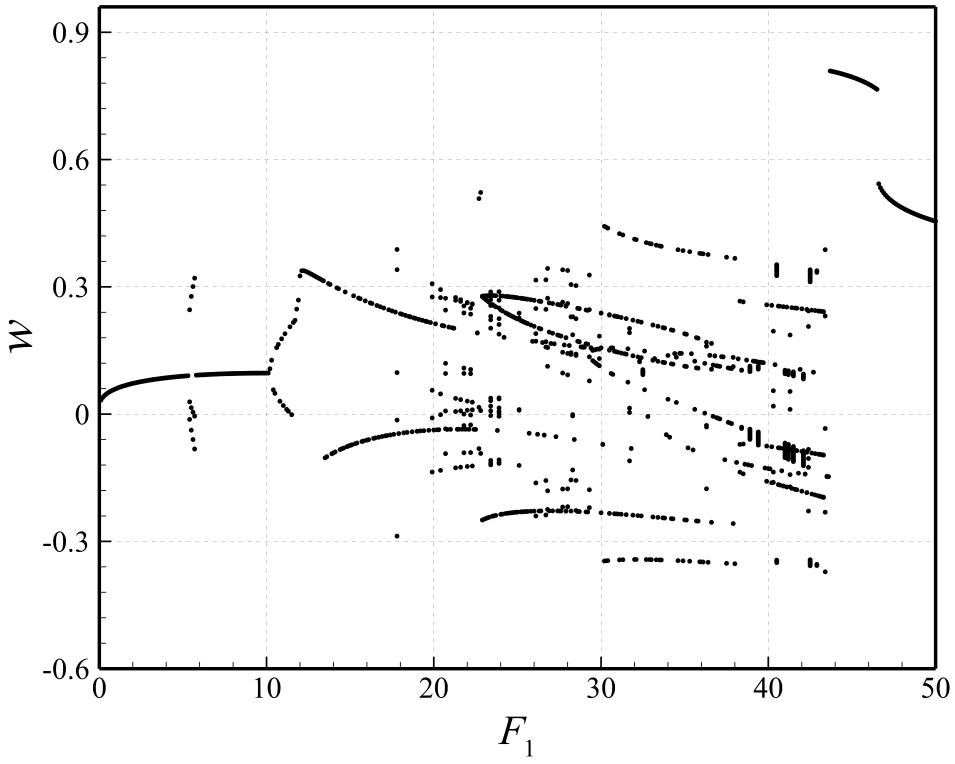

(b)

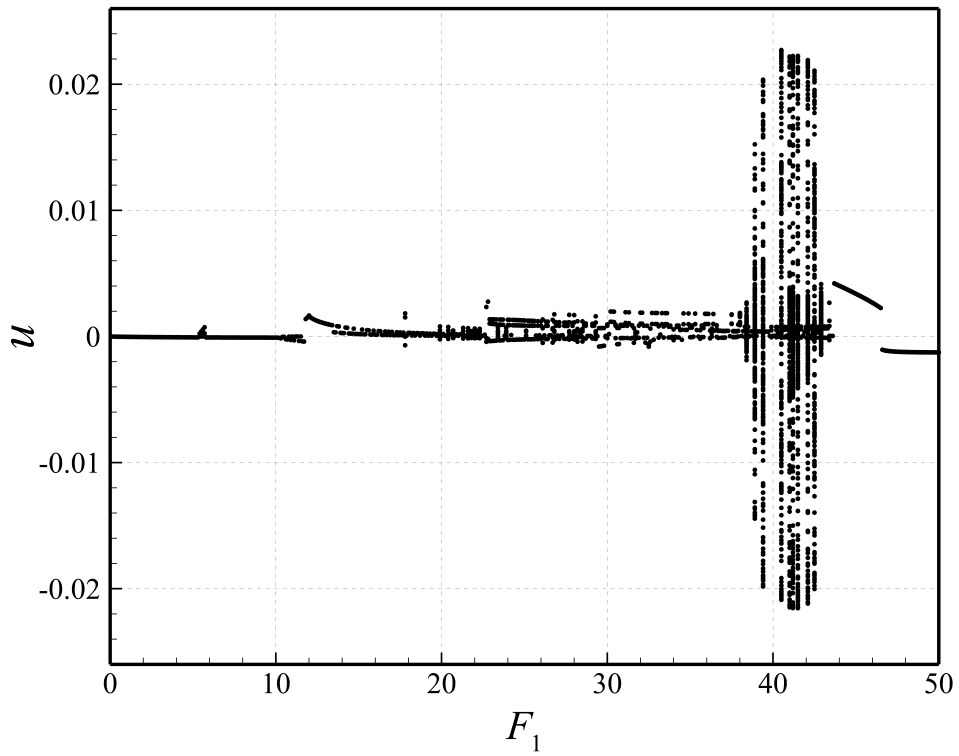

Figure 5: Coupled bifurcation response of the nanoscale tube containing nanofluid flow of speed U = 5.10 for (a) $w(x=0.50)$ and (b) $u(x=0.65)$; ω_1= 3.7896 and ω/ω_1=1.0.

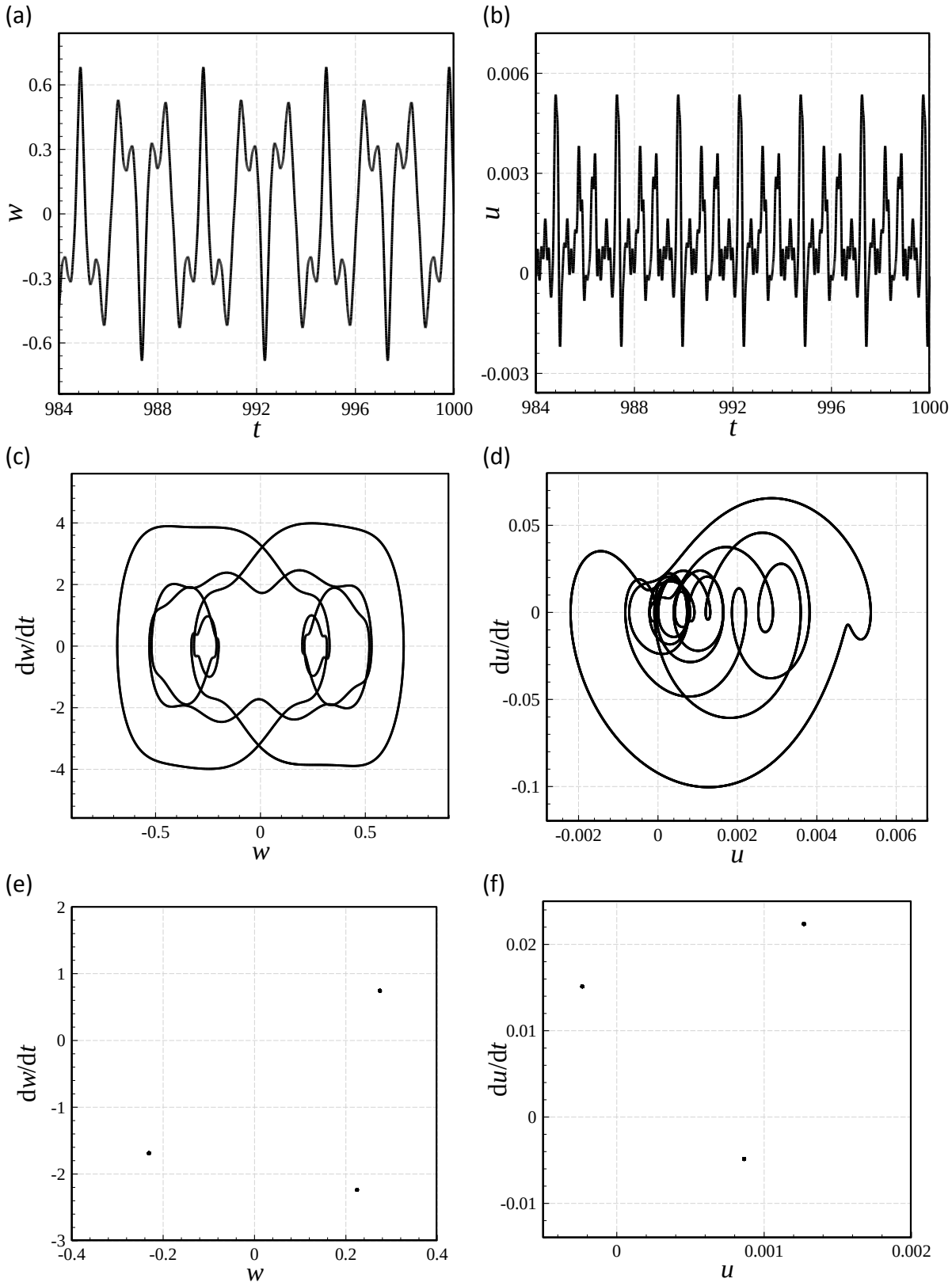

Figure 6: More details about the nanosystem motion (described in Fig. 5) at F_1=25.0: (a) $w(x=0.5)$ versus time, (b) $u(x=0.65)$ versus time, (c) $dw/dt(x=0.5)$ versus transverse displacement, (d) $du/dt(x=0.65)$ versus axial displacement, (e) Poincaré map for $w(x=0.5)$, and (f) Poincaré map for $u(x=0.65)$.

(a)

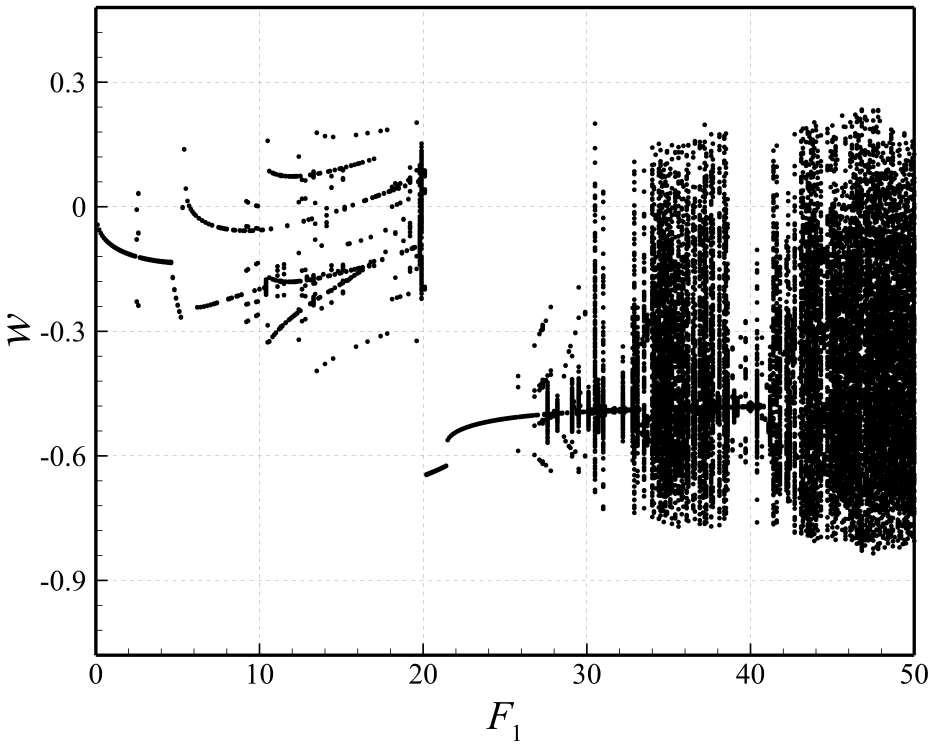

(b)

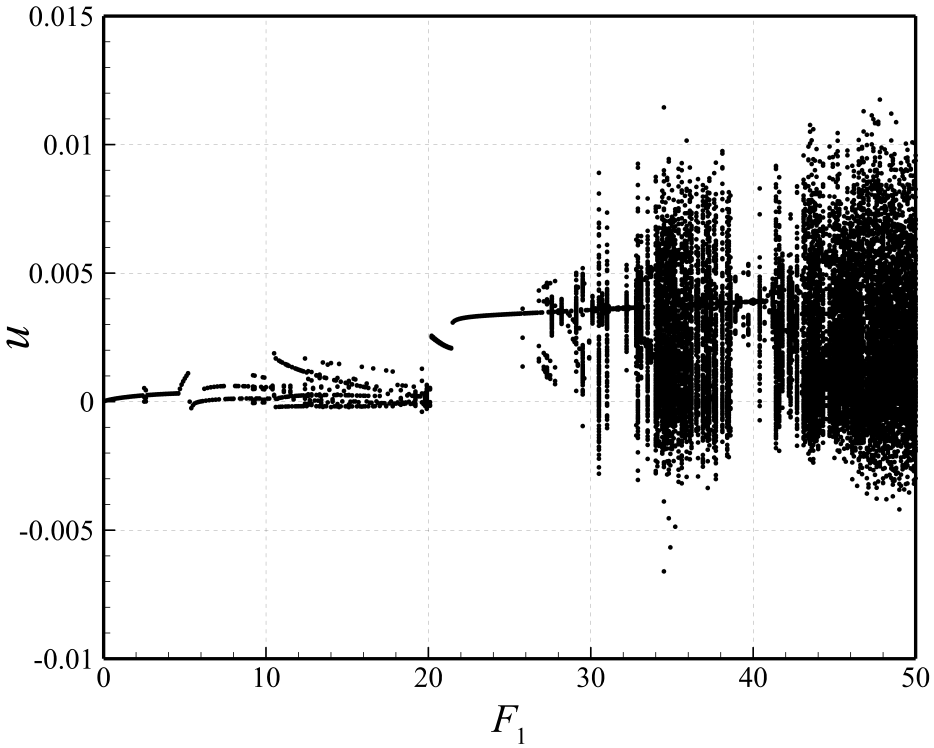

Figure 7: Coupled bifurcation response of the nanoscale tube containing nanofluid flow of speed U = 5.15 for (a) $w(x=0.50)$ and (b) $u(x=0.65)$; ω_1= 2.8935 and ω/ω_1=1.0.

(a)

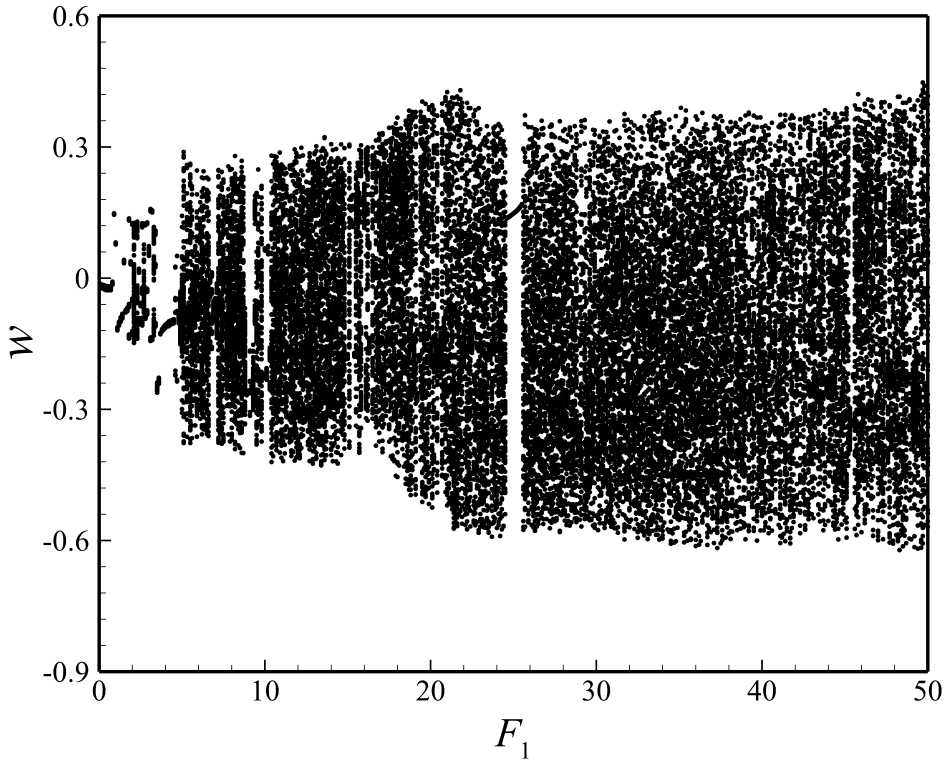

(b)

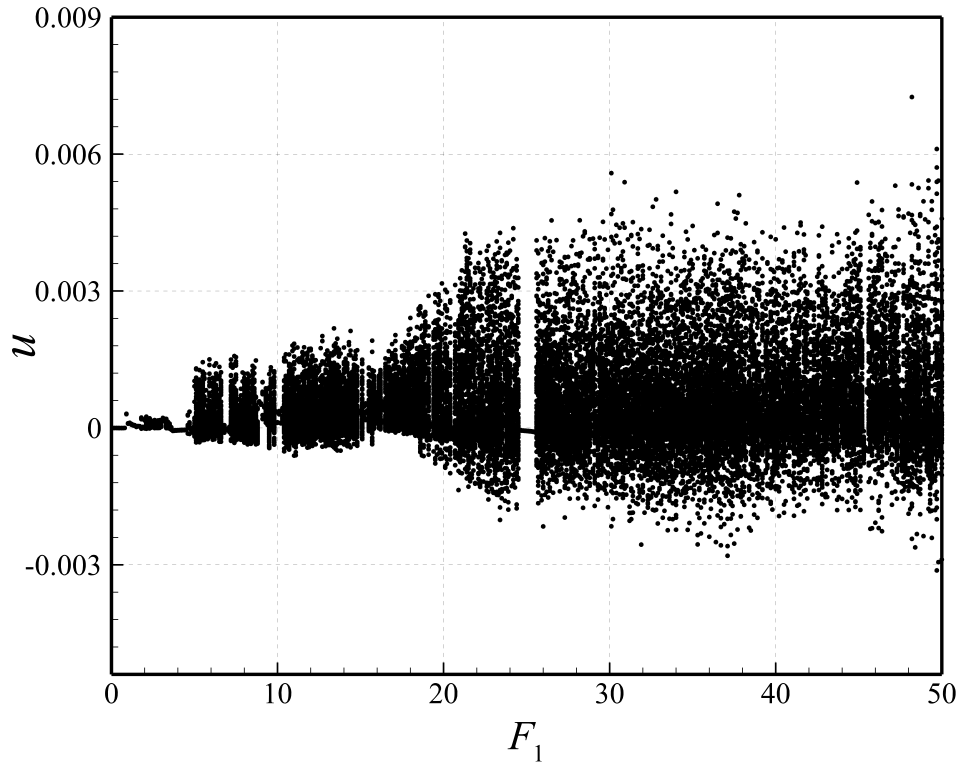

Figure 8: Coupled bifurcation response of the nanoscale tube containing nanofluid flow of speed U = 5.20 for (a) $w(x=0.50)$ and (b) $u(x=0.65)$; ω_1= 1.5772 and ω/ω_1=1.0.

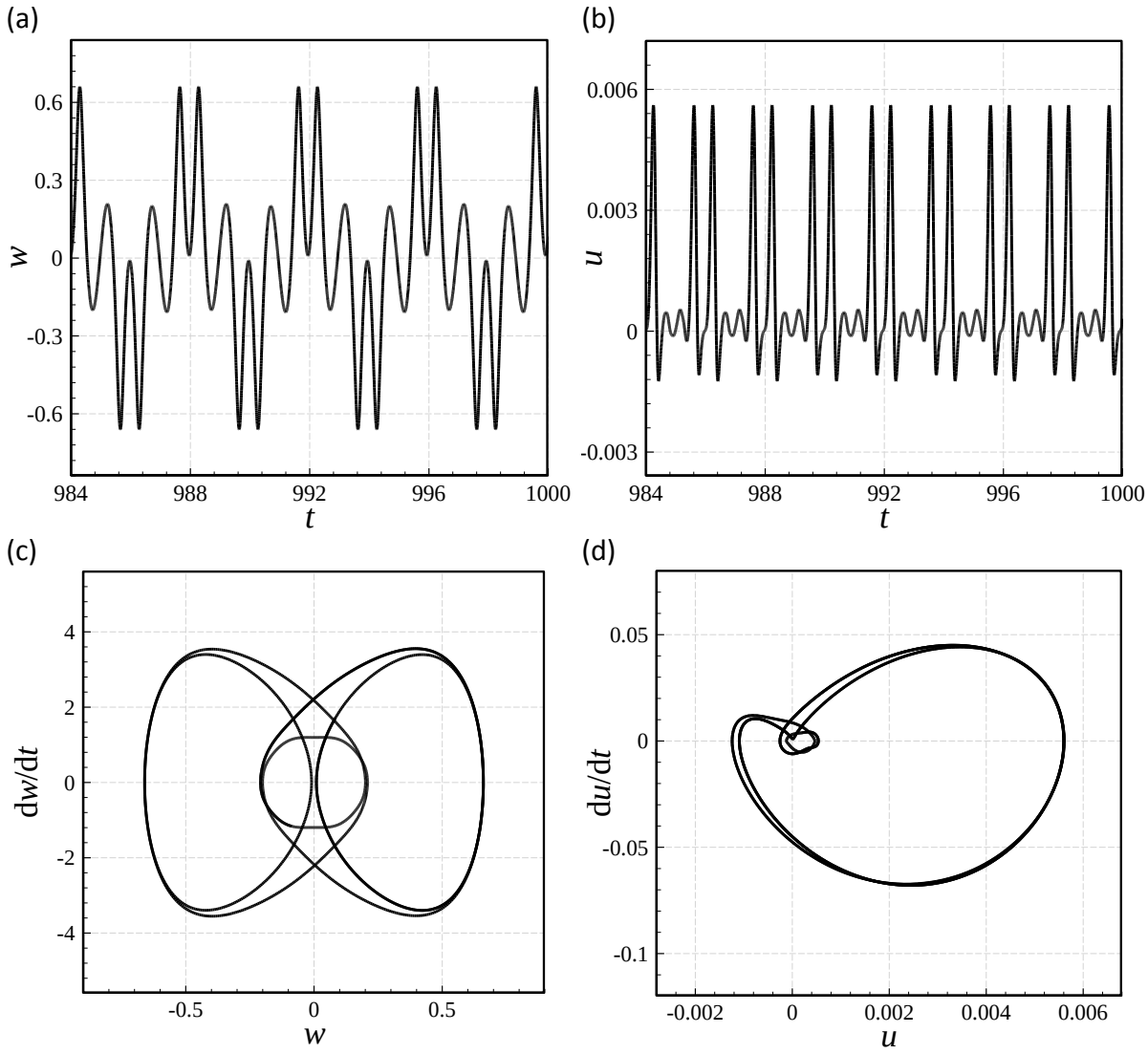

Figure 9: More details about the nanosystem motion (described in Fig. 8) at F_1=25.0: (a) $w(x=0.5)$ versus time, (b) $u(x=0.65)$ versus time, (c) $dw/dt(x=0.5)$ versus transverse displacement, and (d) $du/dt(x=0.65)$ versus axial displacement.

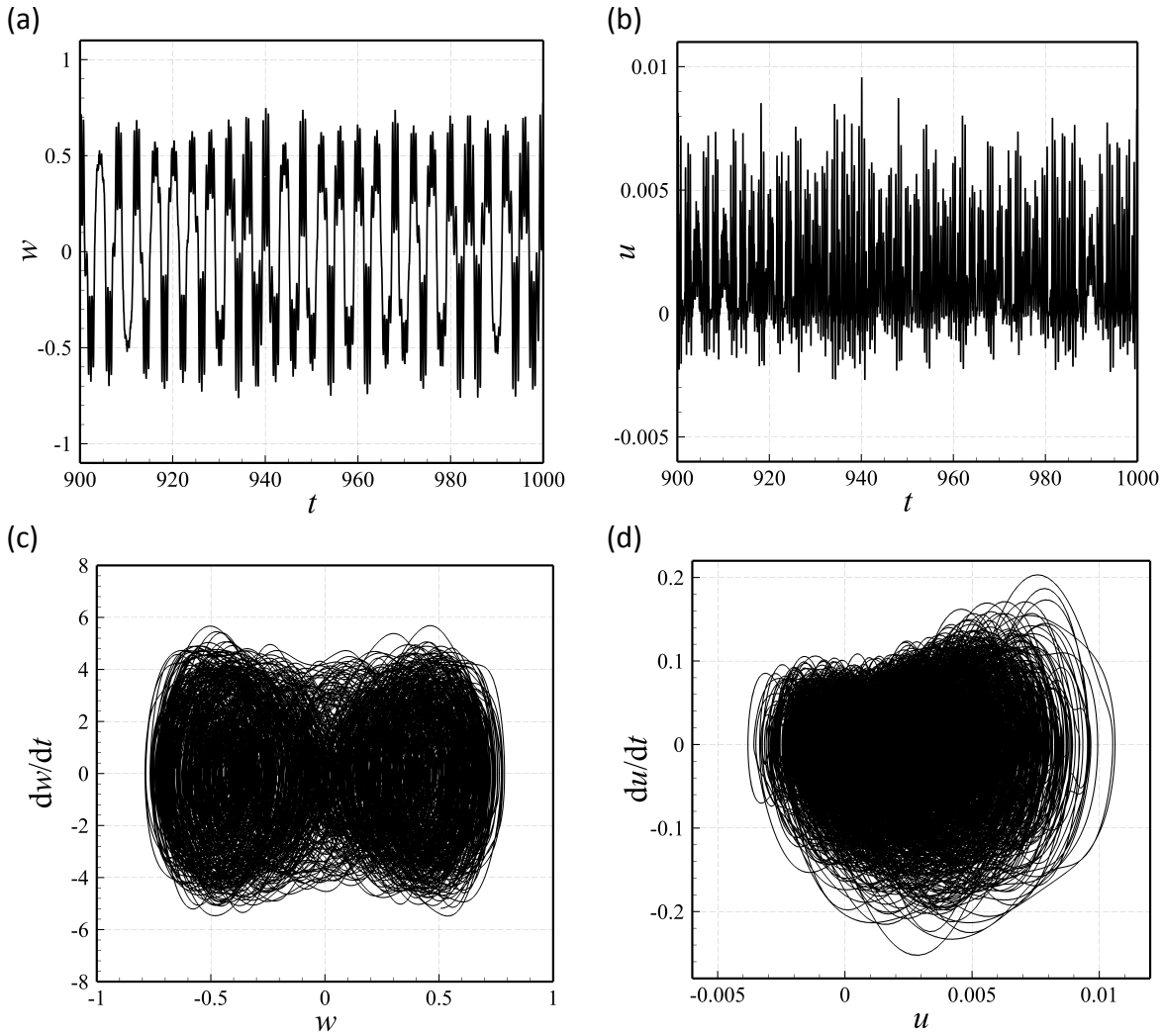

Figure 10: More details about the nanosystem motion (described in Fig. 8) at F_1=38.0: (a) w(x=0.5) versus time, (b) u(x=0.65) versus time, (c) dw/dt(x=0.5) versus transverse displacement, and (d) du/dt(x=0.65) versus axial displacement.

(a)

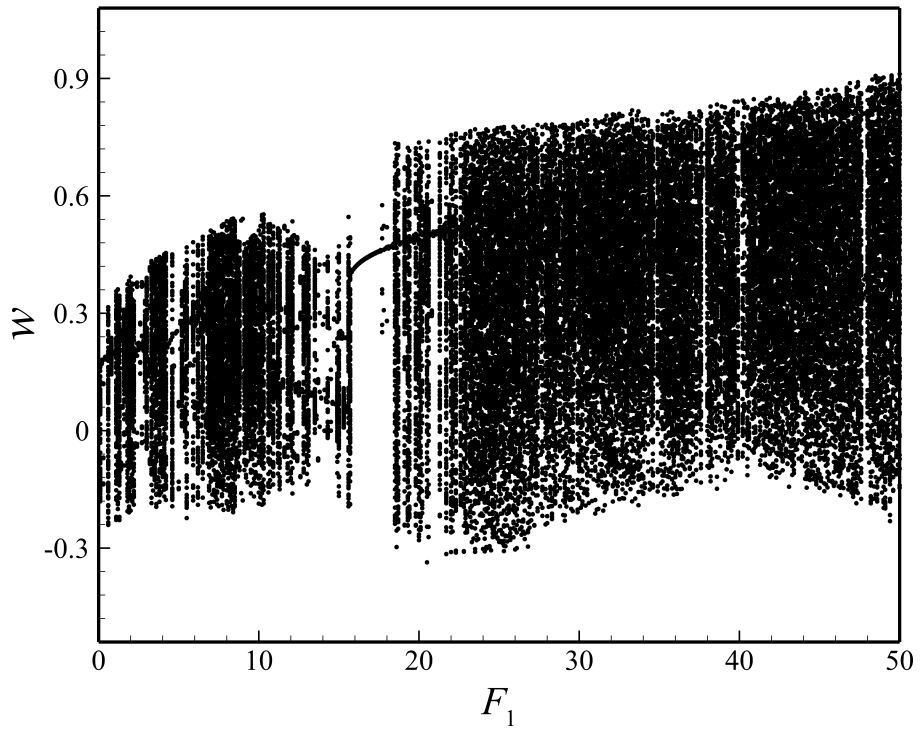

(b)

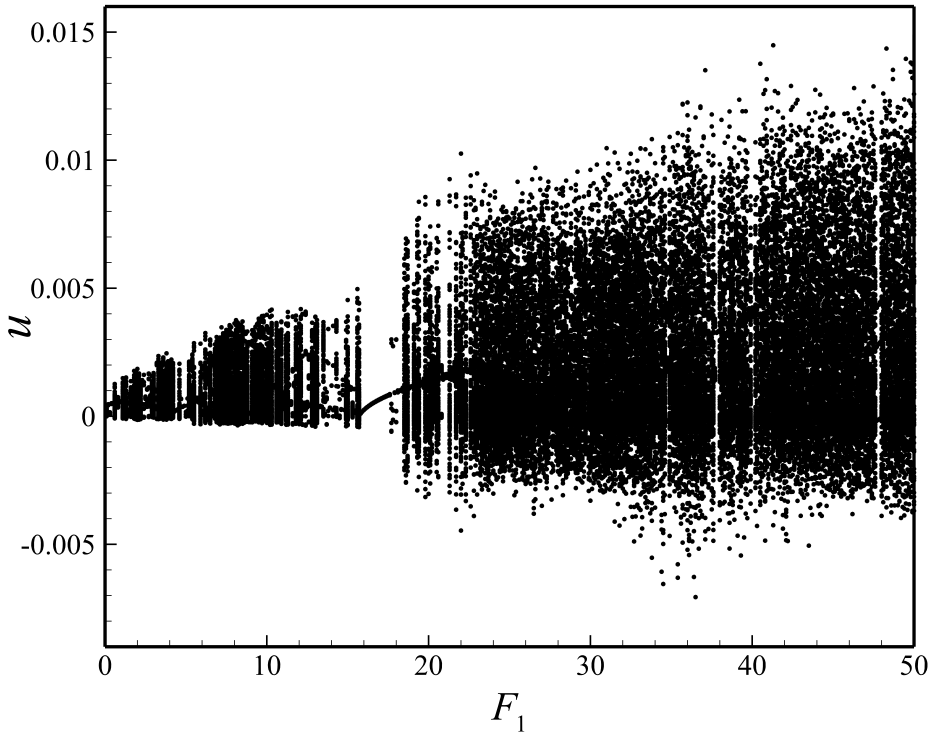

Figure 11: Coupled bifurcation response of the nanoscale tube containing nanofluid flow of speed U = 5.25 for (a) $w(x=0.50)$ and (b) $u(x=0.65)$; ω_1= 2.5663 and ω/ω_1=1.0.

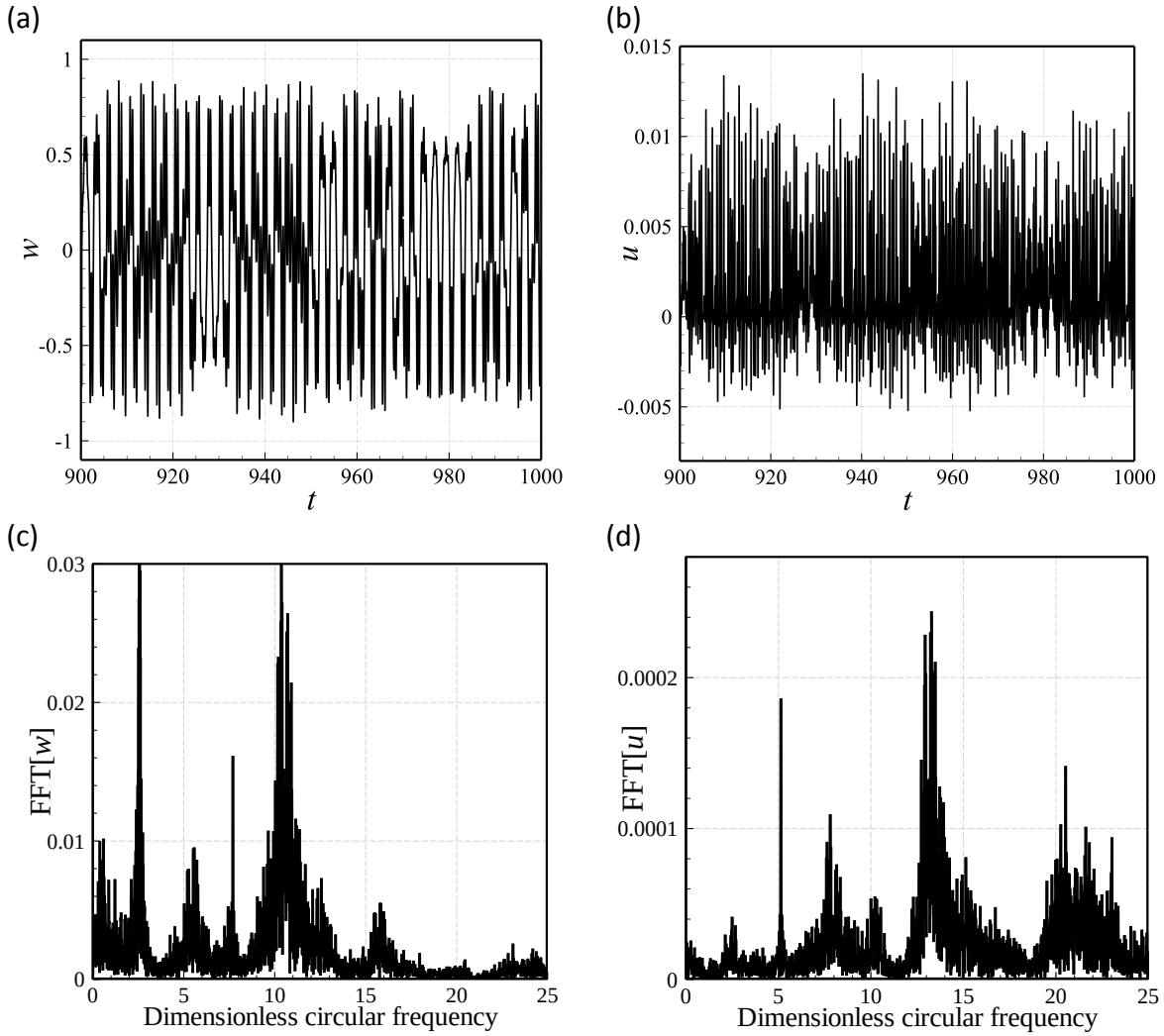

Figure 12: More details about the nanosystem motion (described in Fig. 11) at F_1=46.0: (a) $w(x=0.5)$ versus time, (b) $u(x=0.65)$ versus time, (c) FFT for $w(x=0.5)$, and (d) FFT for $u(x=0.65)$.

(a)

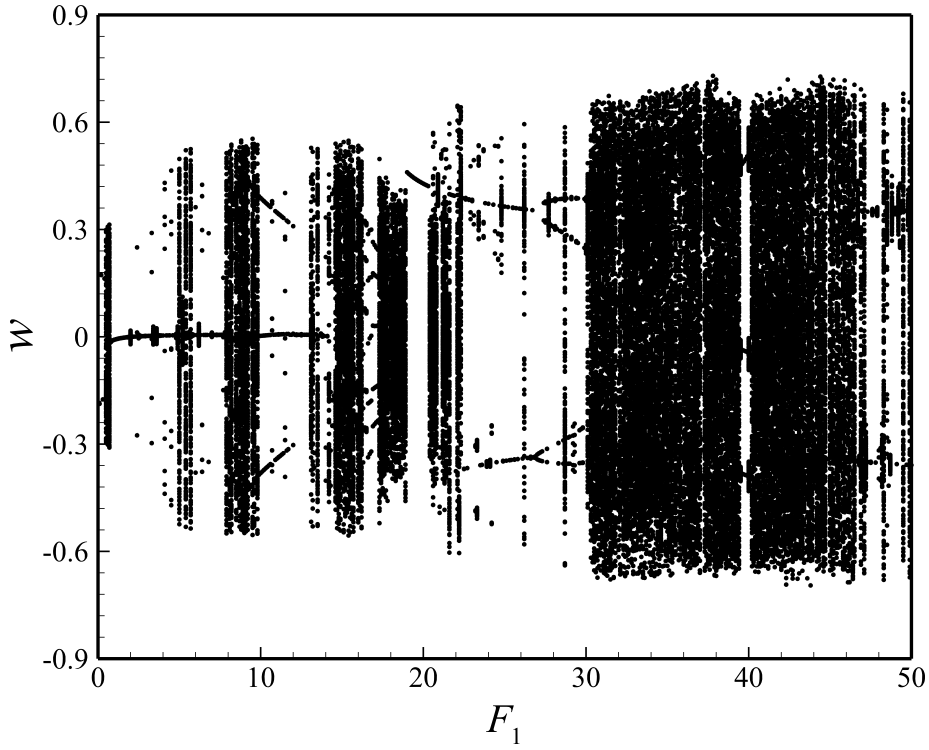

(b)

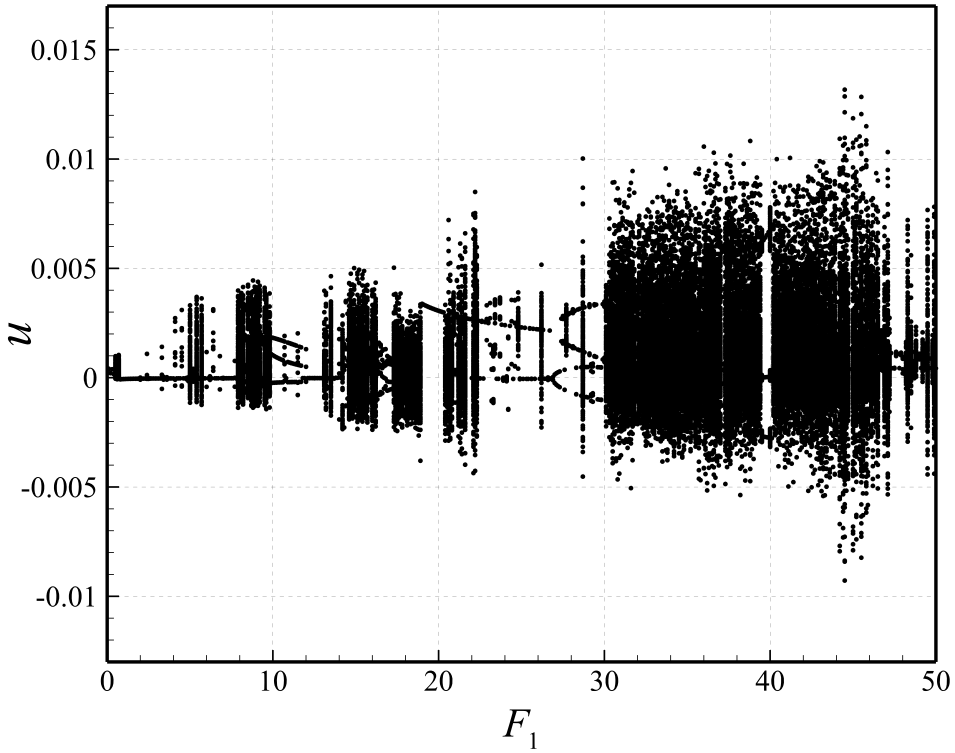

Figure 13: Coupled bifurcation response of the nanoscale tube containing nanofluid flow of speed U = 5.30 for (a) $w(x=0.50)$ and (b) $u(x=0.65)$; ω_1= 4.2434 and ω/ω_1=1.0.

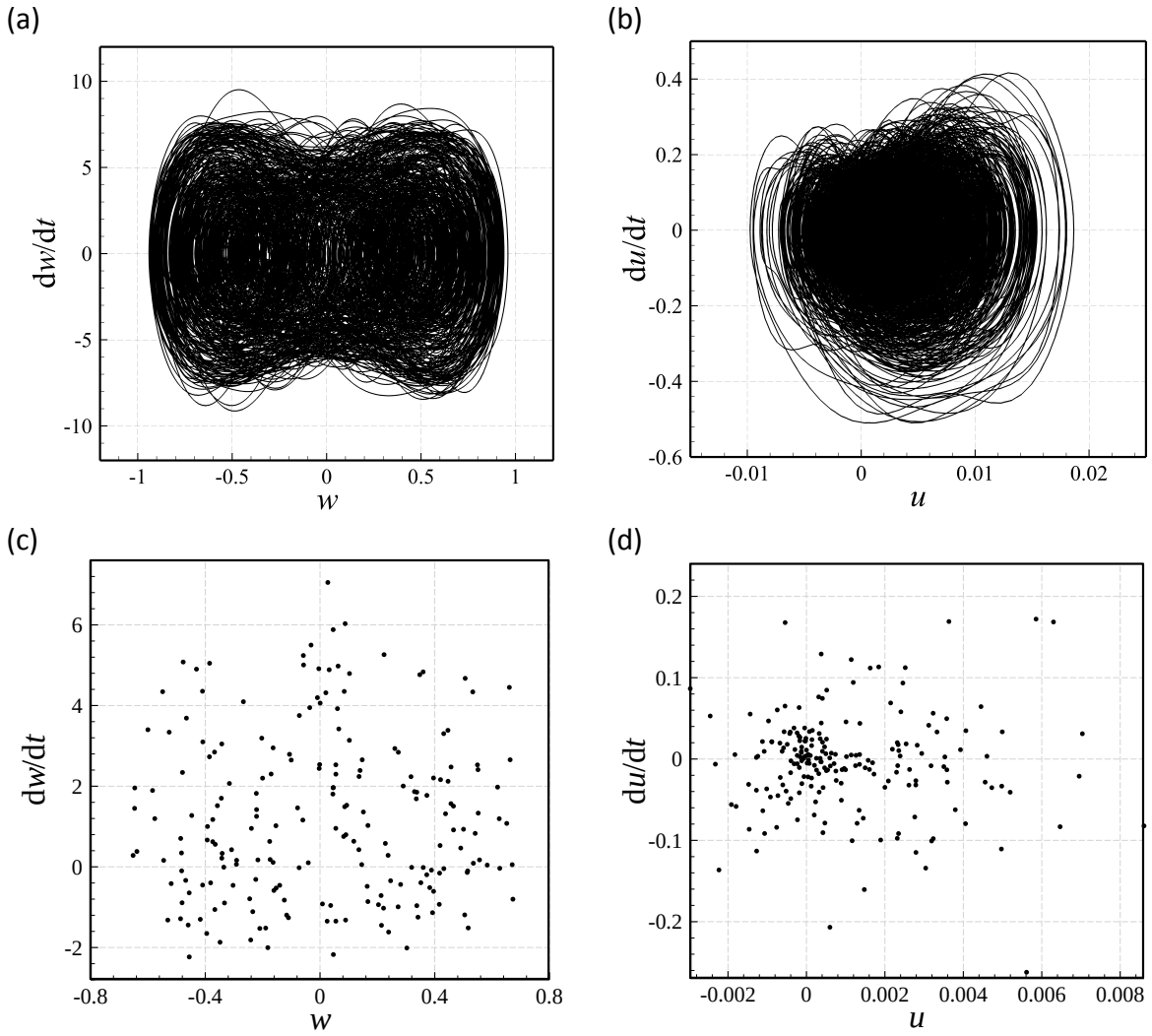

Figure 14: More details about the nanosystem motion (described in Fig. 13) at F_1=42.0: (a) *dw/dt*(*x*=0.5) versus transverse displacement, (b) *du/dt*(*x*=0.65) versus axial displacement, (c) Poincaré map for *w*(*x*=0.5), and (d) Poincaré map for *u*(*x*=0.65).

(a)

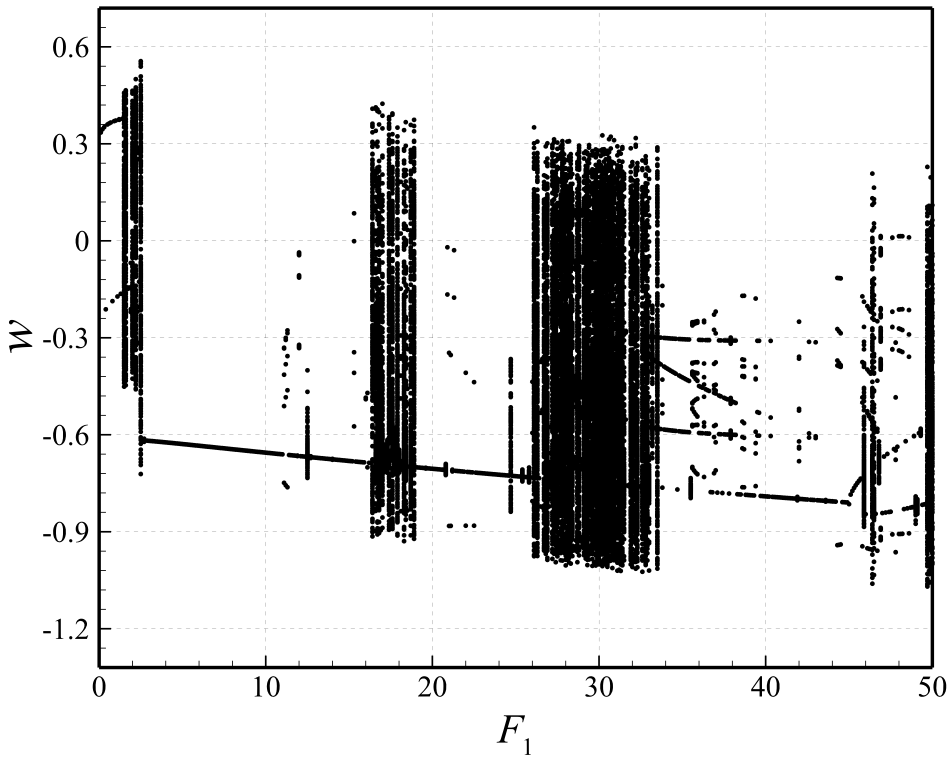

(b)

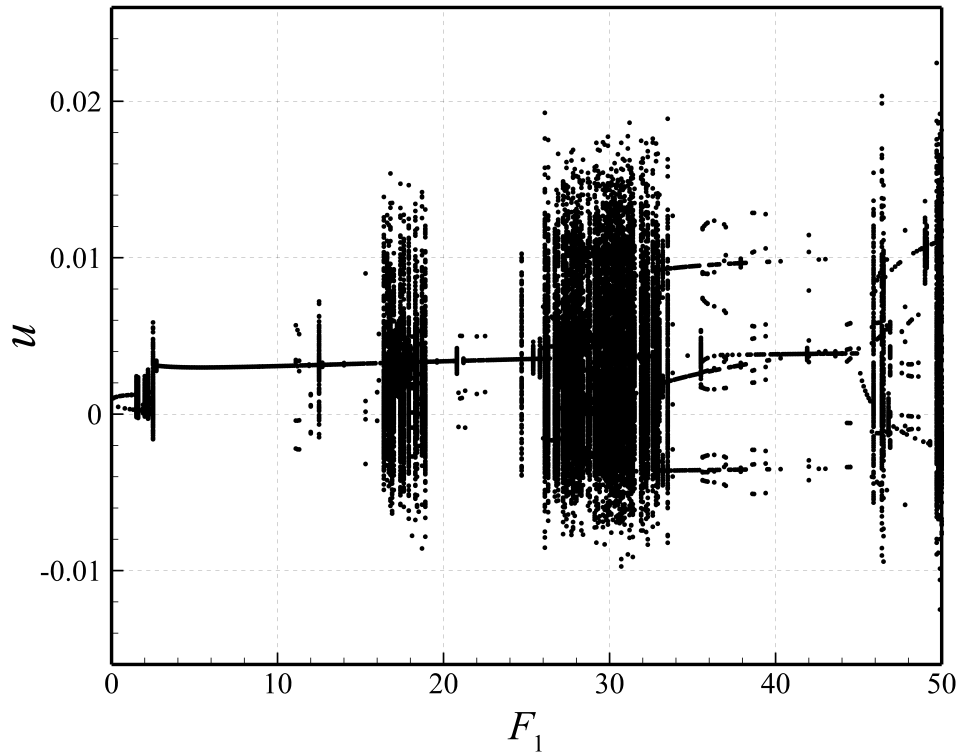

Figure 15: Coupled bifurcation response of the nanoscale tube containing nanofluid flow of speed U = 5.40 for (a) w(x=0.50) and (b) u(x=0.65); ω_1= 6.3597 and ω/ω_1=1.0.